THESIS FOR THE DEGREE OF DOCTOR OF PHILOSOPHY

Modelling of cathode-plasma interaction in short high-intensity electric arc

Application to Gas Tungsten Arc Welding

ALIREZA JAVIDI SHIRVAN

Department of Applied Mechanics
Division of Fluid Dynamics
CHALMERS UNIVERSITY OF TECHNOLOGY
Gothenburg, Sweden 2016

Modelling of cathode-plasma interaction in short high-intensity electric arc

Application to Gas Tungsten Arc Welding

ALIREZA JAVIDI SHIRVAN

ISBN 978-91-7597-381-4

Doktorsavhandlingar vid Chalmers tekniska högskola
Ny serie nr 4062
ISSN 0346-718X

Department of Applied Mechanics
Division of Fluid Dynamics
Chalmers University of Technology
SE–412 96 Gothenburg
Sweden
Telephone + 46 (0)31 – 772 1000

Typeset by the author using LaTeX.

Chalmers Reproservice
Gothenburg, Sweden 2016

to my family

Modelling of cathode-plasma interaction in short high-intensity electric arc - Application to Gas Tungsten Arc Welding

Alireza Javidi Shirvan

Department of Applied Mechanics
Division of Fluid Dynamics
Chalmers University of Technology

ABSTRACT

In arc welding the quality of the weld is strongly influenced by the thermal history of the workpiece which is itself governed by the electric arc heat source. The models for predicting weld properties thus need a good evaluation of the distribution of the heat input from the arc to the workpiece. To have a predictive model of arc heat source it is necessary to take into account the cathode and its coupling with the plasma. The coupling allows to calculate the temperature and current density distributions along the cathode surface rather than prescribing them. This thesis focuses on the arc-cathode coupling for a plasma assumed to be in local thermal equilibrium. A self-consistent coupling boundary model for high-intensity electric arc on a refractory cathode (thoriated tungsten) was developed accounting for the physics of the sub-layers of the cathode layer and the non-uniformity of the cathode surface physical state. The cathode layer model accounts for the non-equilibria in the cathode layer. It was tested in one-dimensional calculations and then extended to a cathode-plasma coupling boundary condition for gas tungsten arc implemented in OpenFOAM. Different modelling assumptions commonly used for developing the model were questioned and investigated. It was checked that the secondary electron emission is negligible compared to the effect of emitted electrons and ions. It was verified that it is justified to neglect the space charge of emitted electron when calculating the cathode surface electric field. It was verified that Richardson-Dushman electron emission law supplemented with Schottky correction is used within its domain of validity in GTA applications even for low work function emitters. It was shown that the radiative absorption of the cathode surface is not negligible compared to the radiative emission. The cathode layer model was also further developed to take into account the inhomogeneity of the cathode material. It was shown that the cathode inhomogeneity has a significant effect on the size of the arc attachment and consequently on the cathode surface and the plasma temperature. Good agreement was obtained with the measured cathode surface and plasma temperatures without imposing any adjustable parameters. The results showed that the proposed model, which is only based on physical principles, is able to predict the trends observed experimentally.

Keywords: electric arc discharge, sheath, pre-sheath, Knudsen layer, doped refractory cathode, arc-cathode coupling, Gas Tungsten Arc simulation, OpenFOAM.

Acknowledgments

My PhD studies were carried out at University West while I was registered at Chalmers University of Technology, division of Fluid Dynamics. The work was supervised by Assoc. Prof. Isabelle Choquet at University West and Prof. Håkan Nilsson at Chalmers. Isabelle Choquet was in this work financed by KK-foundation in collaboration with ESAB and Håkan Nilsson was financed by the Sustainable Production Initiative and the Production Area of Advance at Chalmers.

I would like to express my sincere gratitude to Isabelle Choquet. I know her when I started my master programme and since then she has been a mentor for me. "Thank you Isabelle, not only for your immense knowledge, guidance and patience during my PhD but also for your continuous support for the past ten years."

Many thanks also to Håkan Nilsson for his professional advises and supports especially on fighting with OpenFOAM and on writing the papers and the thesis.

I am grateful to Prof. Hrvoje Jasak for many helpful discussions on OpenFOAM implementation, to Assoc. Prof. Pierre Freton for interesting discussions on the topic and to Kjell Hurtig for preparing experimental measurements for me although I did not have time to include them in the thesis.

I would like to thank my colleagues at University West for creating a pleasant work environment, particularly, Ingrid Elison, the head of engineering department and Prof. Lars-Erik Svensson, the head of welding technology group at the time. I enjoyed working at PTW and had a great time with my fellows: Almir, Americo, Ana, Anna, Ashish, Camilla, Caroline, Christophe, Corinne, Ebrahim, Emile, Esmaeil, Jack, Joel, Josefine, Leif, Lisa, Tahira, Mahdi, Mohit, Patrik, Per, Petter, Vahid, Victoria and the lasts and the least Ali and Jeroen.

I could have not achieved anything in my life without continuous support of my family. I Thank my parents, Parvin and Mohsen, for providing me everything I needed in my life and for giving me the opportunity to chase my dreams. I also thank my sister, Niki, for her kindness and for being inspiring for me."

Above all my deepest sense of gratitude goes to my beloved wife for her constant support. "Salma I could have not done this dissertation without your encouragement, patience and unwavering love."

Alireza Javidi Shirvan
Göteborg, May 2016

List of publications

This thesis consists of an extended summary and the following appended papers:

Paper I

A. Javidi Shirvan, I. Choquet. "A review of cathode-arc coupling modeling in GTAW", *Welding in the World*, 15 pages, (2016).

Division of work: Javidi Shirvan did the bibliography and wrote the paper. Choquet participated to the bibliographic study, wrote some parts of the paper, supervised the planning and organized the writing. Both authors proofed the final paper.

Paper II

A. Javidi Shirvan, I. Choquet. "Modelling of electrode-arc coupling in electric arc welding", *The 6th International Swedish Production Symposium*, 8 pages, (2014).

Division of work: Javidi Shirvan implemented the model, produced all the numerical results and wrote the paper. Choquet wrote some parts of the paper, supervised the planning, the calculations and the analysis and organized the writing. Nilsson supervised the calculations. All authors proofed the final paper.

Paper III

A. Javidi Shirvan, I. Choquet, H. Nilsson, H. Jasak. "Coupling boundary condition for high-intensity electric arc attached on a non-homogeneous refractory cathode", *Submitted for journal publication*.

Division of work: Javidi Shirvan implemented the coupling boundary condition, produced all the numerical results and wrote the paper. Choquet implemented the Murphy Good emission model, wrote some parts of the paper, supervised the planning, the calculations and the analysis and also organized the writing. Nilsson supervised the calculations. Jasak supervised the implementation of the coupling boundary condition in OpenFOAM. All authors proofed the final paper.

Paper IV

A. Javidi Shirvan, I. Choquet, H. Nilsson. "Effect of cathode model on arc attachment for short high-intensity arc on a refractory cathode", *Submitted for journal publication*.

Division of work: Javidi Shirvan implemented the model, produced all the numerical results and wrote the paper. Choquet wrote some parts of the paper, supervised the planning, the calculations and the analysis and organized the writing. Nilsson supervised the calculations. All authors proofed the final paper.

List of additional relevant publications

Relevant publications which are not included in this thesis are listed as the following:

Publication A

I. Choquet, H. Nilsson, A. Javidi Shirvan, "Numerical simulation of Ar-x CO_2 shielding gas and its effect on an electric welding arc", *IIW Commission XII/SG 212 Intermediate meeting, University West, Trollhä ttan, Sweden* (2011).

Publication B

I. Choquet, A. Javidi Shirvan, H. Nilsson. "Electric welding arc modeling with the solver OpenFOAM - A comparison of different electromagnetic models", *International Institute of Welding Document No 212-1189-11.*, (2011).

Publication C

A. Javidi Shirvan, I. Choquet, H. Nilsson, "Numerical modelling of shielding gas flow and heat transfer in laser welding process", *Proceedings of The 5th International Swedish Production Symposium, Linköpping, Sweden*, (2012).

Publication D

I. Choquet, A. Javidi Shirvan, H. Nilsson. "On the choice of electromagnetic model for short high-intensity arcs, applied to welding", *Journal of Physics D: Applied Physics 45(20)*, (2012).

Publication E

A. Javidi Shirvan,. "Modelling of Electric Arc Welding: arc-electrode coupling", Thesis for the degree of licentiate of engineering *Chalmers University of Technology, Gothenburg, Sweden*, (2013).

Nomenclature

A_0	Richardson constant
$\mathbf{A}$	magnetic potential vector
$\mathbf{B}$	magnetic field vector
C_p	plasma specific heat at constant pressure
$E^{c/s}$	electric field at the cathode surface (or cathode/sheath interface)
E_i	ionization energy of the impact ionization reaction
$\bar{E}_i$	average ion recombination energy at the cathode surface
e	electron elementary charge
$\mathbf{E}$	electric field vector
g_j	degeneracy of the energy level ε_j
h	plasma specific enthalpy
h_p	Planck constant
$j^{c/s}$	current density at the cathode surface (or cathode/sheath interface)
j_{em}	electron current density emitted by the cathode
$\mathbf{j}$	current density vector
k_b	Boltzmann constant
m_e	electron mass
m_i	ion mass
$n_{Ar^{l+}}^{p/ps}$	number density of the ion Ar^{l+} at the plasma/pre-sheath interface
$n_{Ar^{l+}}^{s/ps}$	number density of the ion Ar^{l+} at the sheath/pre-sheath interface

$n_e^{p/ps}$	electron number density at the plasma/pre-sheath interface
$n_e^{s/ps}$	electron number density at the sheath/pre-sheath interface
$n_i^{s/ps}$	ion number density at the sheath/pre-sheath interface
P	pressure
$Q_{Ar^{l+}}$	internal partition function of the heavy particle Ar^{l+}
Q_{rad}	plasma radiation heat loss
$q^{cl \to c}$	net heat flux from the cathode layer to the cathode surface
q_{bd}	electron back diffusion energy flux towards the cathode surface
q_{em}	electron energy flux from the cathode surface
q_i	ion energy flux towards the cathode surface
q_{rad}^{abs}	radiative absorption at the cathode surface from the plasma
q_{rad}^{em}	radiative emission at the cathode surface
q_{sem}	secondary electron energy flux from the cathode surface
T^c	cathode temperature
T^p	plasma temperature
$T^{c/s}$	temperature at the cathode surface (or cathode/sheath interface)
$T^{p/cl}$	plasma temperature condition at the cathode layer boundary
T_m	melting temperature
T_v	vaporization temperature
$T_e^{s/ps}$	electron temperature at the sheath/pre-sheath interface
$T_h^{s/ps}$	heavy particle temperature at the sheath/pre-sheath interface
U^s	sheath voltage drop
$\mathbf{u}$	plasma velocity vector
$V^{c/cl}$	cathode electric potential condition at the cathode layer boundary
$V^{p/cl}$	plasma electric potential condition at the cathode layer boundary

v_B	Bohm velocity
$v_{\pm}$	maximum/minimum ion velocity at the cathode surface
v_e	electron thermal velocity
v_i	ion thermal velocity
Z	average ion charge
ΔE_l	lowering of the ionization energy for the ion species l
ϵ_o	permittivity of free space
γ	coefficient of secondary emission
κ	thermal conductivity
κ^c	cathode thermal conductivity
κ^p	plasma thermal conductivity
λ_D	Debye length
λ_R	material specific factor
μ	plasma viscosity
μ_o	permeability of free space
ϕ	work function
ϕ_{eff}	effective work function
ψ	view factor angle
ρ	plasma density
σ	electric conductivity
σ^c	cathode electric conductivity
σ^p	plasma electric conductivity
ε_j	energy of the discrete level j
φ_{bd}	electron back diffusion flux through the sheath
φ_{em}	electron emission flux through the sheath

φ_{em}^{MG}	φ_{em} according to Murphy-Good law
φ_{em}^{RD}	φ_{em} according to Richardson-Dushman law
φ_i	ion flux through the sheath
φ_{sem}	secondary electron emission flux through the sheath

Contents

Abstract i

Acknowledgments iii

List of publications v

List of additional relevant publications vii

Nomenclature ix

Contents xiii

1 Introduction 1
- 1.1 Background . . . 1
  - 1.1.1 Man-made electric discharges . . . 1
  - 1.1.2 Short high-intensity electric arc applied to welding . 3
- 1.2 Motivation . . . 6
- 1.3 Previous work . . . 7
- 1.4 Thesis objectives . . . 11
- 1.5 Methodology . . . 11

2 Physics and modelling 13
- 2.1 Physics of the cathode . . . 13
- 2.2 Cathode emission model . . . 14
- 2.3 Physics of the cathode layer . . . 16
  - 2.3.1 Sheath (space charge layer) . . . 17
  - 2.3.2 Knudsen layer . . . 17
  - 2.3.3 Pre-sheath (ionization layer) . . . 17
- 2.4 Main cathode layer modelling assumptions . . . 18
- 2.5 System of equations . . . 19

3 Numerical procedures **21**
3.1 Local numerical procedure 21
3.2 Global numerical procedure 22
3.3 Dynamic arc attachment 23
3.3.1 Surface element without arc attachment 23
3.3.2 Surface element with arc attachment 24

4 Summary of the results **27**
4.1 Cathode layer model results 27
4.2 Verification of assumptions 31
4.3 Comparison to temperature measurements 35

5 Concluding remarks **39**
5.1 Future work 41

6 Summary of papers **43**
Paper I 43
Paper II 44
Paper III 44
Paper IV 45

References **47**

Appendices **53**

A - Equations and derivations **55**
A-1 Cathode layer model derivations 57
A-1.1 Main assumptions 57
A-1.2 Plasma composition in the pre-sheath 58
A-1.3 Flux components in the cathode layer 60
A-1.4 Charge and energy conservation 66
A-2 Equations governing the cathode and the plasma 73

B - Appended Papers I-IV **75**
Paper I 77
Paper II 105
Paper III 115
Paper IV 155

Chapter 1

Introduction

Electric arc discharges, and more specifically gas tungsten arcs (GTA) applied to welding, are complex fluid mechanics problems involving thermal and electromagnetic phenomena. The thesis is started by introducing the general background about man-made electric arcs and more specifically the electric arcs applied to welding (Section 1.1). The motivation of this study is then presented (Section 1.2) and the previous works on the modelling of the electric arc discharge are summarized (Section 1.3). Then the thesis objective is addressed (Section 1.4). Finally the methodology used to achieve the thesis objective is described (Section 1.5).

1.1 Background

An electric arc is a specific type of electric discharge. An electric discharge can form in a media that is usually electrically non-conductive. A familiar example existing in nature is the lightening. It can initiate, for instance, when the electric potential difference between the top and bottom of a cloud goes beyond the breakdown voltage of the media. The electric resistance of the media suddenly drops down and the electrically insulating media becomes conductive. The gas then turns into a plasma. The current intensity of a lightning stroke is around 50000 Amperes. Man-made discharges are much more modest in terms of current intensity than the common natural discharges.

1.1.1 Man-made electric discharges

A simple way of making an electric discharge over a large range of current was developed by John Townsend. It consists in applying a voltage, V, between two planar electrodes located in a glass tube filled with a gas such as argon. When increasing the applied voltage an increasing number of

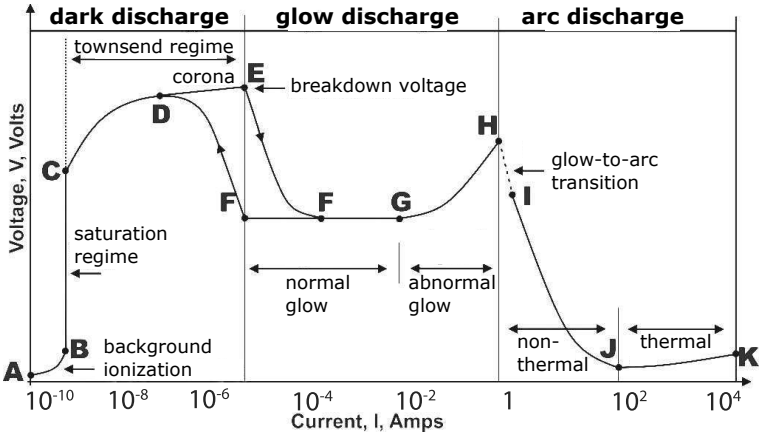

Figure 1.1: The main characteristic curve of the electric discharge (non-specified gas) [1]

electrons are extracted from the cathode. The electrons are attracted by the anode and migrate towards it, creating an electric current, I, in the tube. Three types of discharges may be successively observed when increasing the current intensity, i.e. the dark, the glow and the arc discharge. All of them can be used for a broad variety of applications. As shown in Fig 1.1 each type of discharge can be further divided into subtypes. These subtypes are summarized as follows, where the characteristic data in the brackets corresponds to an argon plasma at atmospheric pressure [15].

1. **The dark discharge**: This type of discharge is non-thermal (or cold). It is not visible to the eye, except for the Corona regime. In a dark discharge, electrons are enough accelerated by the applied potential to initiate ionization reactions as they collide with the gas, and produce secondary electrons. However, they do not gain enough kinetic energy to self-sustain the discharge. Four regimes can be observed:

   - (A-B) Background ionization regime: $(10^{-10} \leqslant I < 10^{-9} A)$
   - (B-C) Saturation regime: $(I = 10^{-9} A)$
   - (C-D) Townsend regime: $(10^{-9} < I < 10^{-5} A)$
   - (D-E) Corona discharge: $(10^{-7} < I < 10^{-5} A)$.

   The dark discharge is, for instance, the operating principle of antistatic applications for plastic films, also of plasma chemistry for producing ozone used to remove bacteria in swimming pools. An electric discharge becomes self-sustained when its voltage reaches

the breakdown voltage. Then, the cathode generates enough electrons to balance the current taken away by the electric discharge. This delimits the transition from dark to glow discharge.

2. **The glow discharge:** This type of discharge is visible but non-thermal since the energy of the ions and molecules remains much lower than the electron energy (for ions and molecules the temperature is of the order of room temperature). Two regimes can be observed:

   - (E-G) Normal glow regime: $(10^{-5} \leqslant I < 10^{-2}A)$
   - (G-H) Abnormal glow regime: $(10^{-2} \leqslant I < 1A)$.

   Man-made glow discharges are used to make plasma-screen television, and fluorescent lights. They can also be used for instance for depositing thin films and doping micro-electronics components.

3. **The arc discharge:** This type of discharge is visible and can be thermal or non-thermal. In the thermal case, the temperature is of the order of 10^5 K. This high temperature is however low compared to the temperature of a star for instance. For this reason, electric arcs are also classified in the family of cold plasmas, while a star is a hot plasma. Two regimes can be observed:

   - (H-J) Non-thermal regime: $(0.1 \leqslant I < 10A)$
   - (J-K) Thermal regime: $(I \geq 10A)$.

The arc discharges in the thermal regime (or a thermal arcs) are often coupled with a gas flow to form plasma jets with temperatures above the melting point of many metals and ceramics. They are thus commonly used for material processing such as plasma cutting, thermal plasma spray and arc welding.

According to the description above, electric arcs applied to welding are in the frame of cold plasma and the discharge type is the thermal arc discharge. To be more specific, they belong to the high-intensity discharges (of the order of 100 A) with short arcs (a few millimeters between the anode and the cathode).

1.1.2 Short high-intensity electric arc applied to welding

Some of the main arc welding processes are illustrated in Fig 1.2 and briefly described here. In the standard welding nomenclature, the pieces to be joined are referred to as the workpiece. The workpiece acts as

either a cathode or an anode depending on the type of application. The molten part of the workpiece is referred to as the weld pool. The electrode with the other polarity, mounted into a welding torch, is referred to as the electrode. The arc welding tools can be divided into two different categories: those with consumable (non-refractory) electrode and those with non-consumable (refractory) electrode.

Arc welding with consumable electrode

A consumable electrode is characterized by a low melting temperature. Its tip melts during arcing and forms droplets that are transferred to the weld pool. The electrode is then continuously fed forward into the arc. Shielding is needed to protect the molten metal from oxidation. When the shielding is provided by a gas, which is injected through the welding torch, the process is called gas metal arc welding (GMAW), see Fig 1.2(a). If the

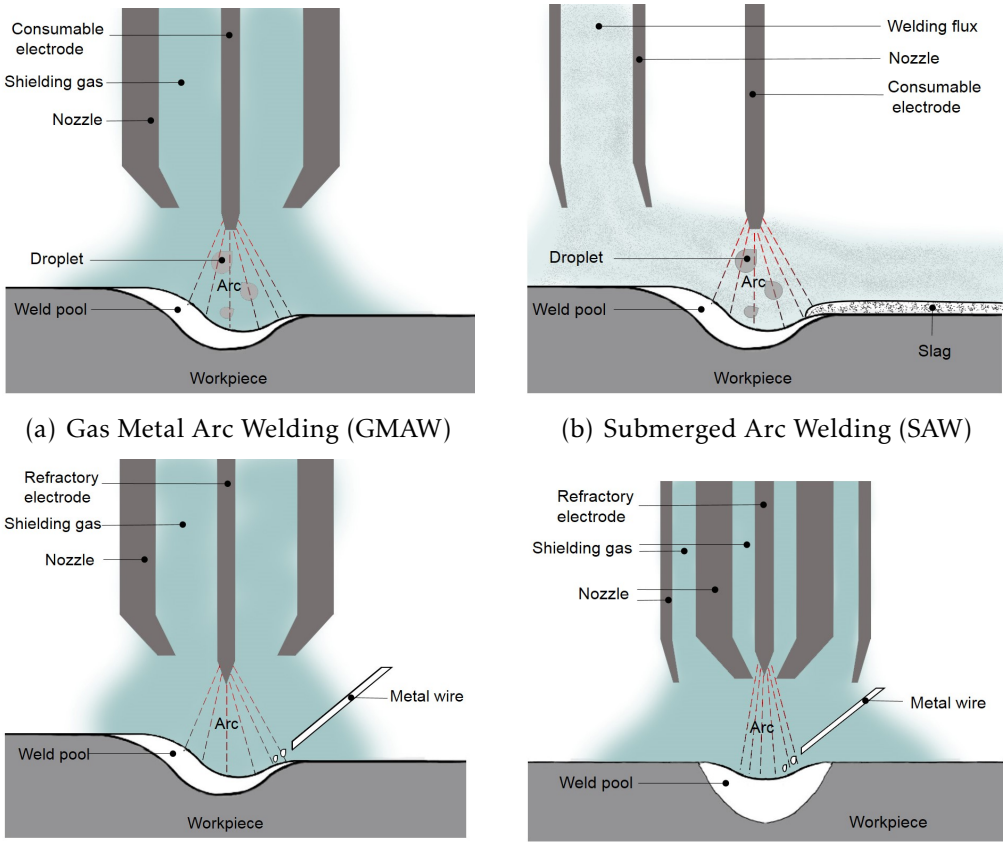

(a) Gas Metal Arc Welding (GMAW)

(b) Submerged Arc Welding (SAW)

(c) Gas Tungsten Arc Welding (GTAW)

(d) Plasma Arc Welding (PAW)

Figure 1.2: Schematic sketch of four different types of electric arc welding processes.

shielding gas is inert (i.e. a rare gas or a mixture of rare gases) the process is called metal inert gas (MIG), and if an active gas is employed it is called metal active gas (MAG). For a given power input, the arc temperature obtained with an active gas uses to be higher than with an inert gas. The power supply is direct current (DC) in which the electrode is normally connected to the positive pole.

Submerged arc welding (SAW) is another type of welding which can be performed with multiple or with a single consumable electrode (see Fig 1.2(b)). The arc is then submerged in a blanket of welding flux. The welding flux is granular fusible flux made of carbonate and silicate material which is melted and partially vaporized by the electric arc. The molten flux is electrically conductive, and provides a current path between the electrode and the workpiece. The flux can also be used to apply alloying element to the weld pool. The vaporized flux protects the weld from oxidation by pushing away the atmospheric gases. The process can be performed using a DC or an alternative current (AC) power source.

Arc welding with non-consumable electrode

The non-consumable electrodes used in welding are usually made of tungsten. This material is characterized by a high melting temperature. The electrode melting is then negligible. The tungsten is doped with an activator (a rare earth metal oxide) to facilitate arc ignition and promote arc stability. A shielding gas is used to protect the weld pool. If the electrode has the polarity of a cathode, it can emit electrons in the thermionic or in the field enhanced thermionic regime, due to its elevated temperature. The corresponding welding process is called gas tungsten arc welding (GTAW), or tungsten inert gas welding (TIG). A sketch of this process is shown in Fig 1.2(c). The shielding gas supplied by the torch is often inert (e.g. argon or a mixture of argon and helium). Three choices of welding current are possible, depending on the required process properties: direct current straight polarity (DCSP), direct current reverse polarity (DCRP), and alternating current with high frequency stabilization (ACHF). GTAW with DCSP produces deep penetration joints, and has no cleaning action on the workpiece. GTAW with DCRP has a good cleaning action on the surface of the workpiece, but it produces shallow weld joints. GTAW with ACHF alternatively combines the good weld penetration with the cleaning action. The DCSP polarity is the most common. This is the polarity used in this study.

A variant of GTAW is plasma arc welding (PAW), see Fig 1.2(d). Its specificity is to constrict the arc, so that the heat transferred to the workpiece is more localized. It leads to deeper welds compared to GTAW. More

details about different variants of arc welding processes can be found in the books by Weman [57] and Messler and Robert [41].

1.2 Motivation

Material microstructure and mechanical properties mainly govern the quality of the weld. They are strongly influenced by the material composition and the thermal history along the welding process. The thermal history is based on the heat transferred from the arc to the workpiece. The prediction and production of high quality welds require characterizing and controlling the heat source. Therefore, the models for predicting weld properties need a good evaluation of the distribution of the heat input from the arc to the workpiece. It is known from Murphy et al. [43] that an electric arc heat source simplified to an analytic expression of the heat flux to the workpiece is not sufficient to predict reliable weld properties. Characterizing such a heat source is thus a basic requirement. This is addressed in the present study with focus on gas tungsten arc applications. An electric arc heat source can be characterized either experimentally or through modelling and numerical simulation. These two approaches complement each other. Experimental measurements can provide temperature distributions in the arc but they do not yet provide the local distribution of current density nor of heat transfer. The temperature distributions measured experimentally in the arc is however valuable information for validating the models. The simulation models can provide additional information such as the local current density distribution and the heat input into the base metal. The approach used in this study is based on modelling and simulation.

The numerical simulation of a thermal plasma arc can be done considering only the plasma core, and ignoring its coupling with the anode and the cathode [24, 31, 33, 62]. This approach requires that the temperature and the current density distribution are specified at the boundaries. These conditions are very difficult to measure experimentally and a limited number of documented studies are available. An example of plasma temperature measurement by Haddad and Farmer [27] can be seen in Fig 1.3. It was done using spectroscopy of a steady gas tungsten argon arc on a water cooled workpiece. As can be seen the temperature is not accessible to measurement in the vicinity of the cathode and anode surfaces. Therefore, data extrapolations are needed to set the temperature boundary conditions. It is obvious that the extrapolations can be very approximate. Current density distributions were measured by Nestor [46] for a cylindrical cathode with flat-end surface, but to our knowledge such

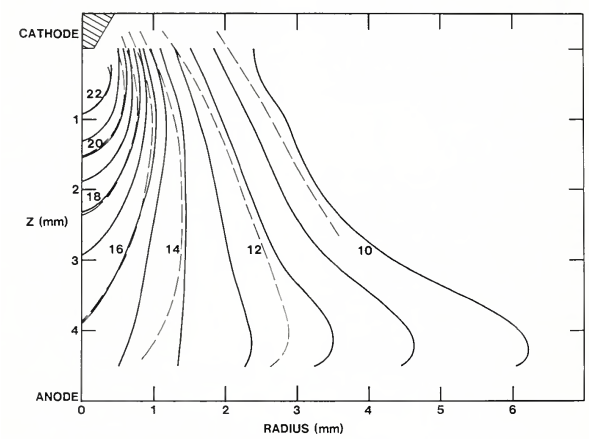

Figure 1.3: Temperature measurement of a GTAW torch burning on a water cooled anode. Dashed lines show results of measurement in an enclosed chamber [27].

measurements are not available for the cathodes with conical tip as used in GTAW. The current density profiles are then assumed to obey analytical distributions scaled to reproduce the total current density. The poor accuracy of these semi-empirical or extrapolated boundary values can have an impact on the calculation results as shown by Choquet et al. [18]. Moreover, this simplified approach cannot be predictive. Therefore, to be able to have a predictive arc heat source model it is necessary to take into account the plasma column, the anode, the cathode and their respective coupling. As this study addresses gas tungsten arcs with direct current straight polarity, the electrode is a cathode. This thesis focuses on the arc-cathode coupling since this is the region where the thermal plasma arc forms. The coupling between the cathode and the plasma allows to calculate the temperature and current density distributions along the cathode rather than prescribing them. This coupling, however, is complex to model due to the non-uniformity of the layer (called cathode layer) between the cathode surface and the plasma core. This field of research is very active. Several approaches were developed before this thesis, and developments took place in parallel to this thesis work too.

1.3 Previous work

Initially the cathode layer models were developed to study the cathode layer region alone. It was done without considering the coupling to the thermal plasma arc nor to the cathode. The first validations by comparison

to experimental measurements were done for high-intensity discharge lamps (HID). HID have a smooth cathode geometry compared to the sharp GTAW cathodes. They are characterized by a lower power and longer anode to cathode distance than gas tungsten arcs. Therefore compared to GTA, they provide lower temperature gradients and larger space for observation. It makes HID lamp easier to be characterized experimentally.

Later works aimed at coupling the cathode layer model to the cathode and the plasma region. The status of cathode layer modelling previous to the present thesis work was the following. It was known that the cathode layer presents several severe non-equilibria including deviations from thermal, ionization and charge equilibrium. It was also known that the charge non-equilibrium implies a cathode layer voltage drop that plays an important role in converting the input electric energy into the output thermal energy. Different cathode layer models based on different physical assumptions were developed. They can be categorized into three different approaches.

- **the diffusion approach** assumes that the voltage drop as well as the thermal non-equilibrium are negligible in the cathode layer. It assumes that the main physical phenomena taking place in the cathode layer for making the transition between cathode and thermal plasma arc is the diffusion of charged particles. This approach was introduced by Lee et al. [37] and further developed by Morrow and Lowke [42].

- **the partial-LTE approach** does the opposite assumptions of the diffusion approach. It models the voltage drop as well as the thermal non-equilibrium and neglects the diffusion of charged particles. This approach was introduced by Zhou et al. [61, 63], and further developed by Coulombe [19] and more recently by Cayla [12].

- **the hydrodynamic approach** takes into account the voltage drop, the thermal non-equilibrium and the diffusion of charged particles. This approach was introduced by Hsu and Pfender [32], further developed by Delalondre [23], and completed by Benilov and co-authors [2, 5–8, 10, 38].

The diffusion approach is very different from the two other approaches. As this approach neglects the cathode layer voltage drop, more specifically the cathode sheath voltage drop, the electron emission is purely thermionic and cannot be field enhanced. Also the electrons and ions cannot be accelerated by the sheath voltage drop in order to convey energy from the electric field to the thermal plasma (see Section 2.3 for more

description of the cathode sub-layers). This is however the basic operating principle of a cathode layer. The diffusion approach models this energy transfer in another way. It provides a non-equilibrium composition of the cathode layer based on ambipolar diffusion induced by the ion flux towards the cathode. It results in an electron density larger than the local thermal equilibrium (LTE) density in the cathode vicinity, and thus promotes current flow via diffusion. Electrons and ions are thus accelerated by a potential fall induced by the ambipolar diffusion. However, as this ambipolar potential fall is low, the electrons cannot be accelerated up to a kinetic energy large enough to ionize the media and self-sustain the discharge. The discharge is instead sustained by the diffusion-promoted current flow and the resultant Joule heating. In other words this model provides a transfer of electric energy into thermal energy due to ambipolar diffusion, while in a cathode layer this is due to the formation of a space charge layer inducing a cathode voltage drop in front of the cathode surface. It is also known from experimental measurements of high-intensity arcs that the cathode layer voltage drop is not negligible compared to the arc column voltage. They are indeed of the same order of magnitude [32].

The partial-LTE approach and the hydrodynamic approach are able to model the physics of the cathode layer using basic principles such as energy and charge conservation. They include the cathode sheath voltage drop and thus are able to take into account the acceleration of the electrons in the sheath that provides them with enough energy to promote impact ionization. The physics of the hydrodynamic approach is more complete since it also takes into account the diffusion of charged particles. It however uses the cathode surface temperature and the cathode layer voltage drop as inputs. These quantities are the unknowns of the cathode layer model. Therefore it imposes extra numerical resolutions. As a result, when making the coupling with the cathode and the plasma, the cathode layer model is not solved locally along the cathode surface and spatial uniformity is assumed along the cathode surface. It is also desynchronized which means that it is not updated as often as the systems of equations in the cathode and the plasma [4]. These simplifications are accepted for HID applications but they might be questioned when considering GTA since distributions along a GTA cathode tip are not uniform. On the other hand, the input to the partial-LTE approach (developed by Cayla [12]) is the current density on the cathode surface, which is provided by the cathode model. This choice is thus more suited for a local and synchronized solution of the cathode layer model.

Previous to the present thesis work, some of these models were applied to simulations of high-intensity electric arcs. The most complete cathode

layer model of the partial LTE approach, developed by Cayla, and the most complete cathode layer model of the hydrodynamic approach, developed by Benilov, had been applied to HID lamps. However, none of the partial-LTE nor the hydrodynamic approach had been applied to GTA. The only applications to GTA had been done within the frame of the diffusion approach, first by Zhou et al. [64] and then by other authors [40, 52, 65].

In parallel to the present thesis work, Beava et al. [3, 4, 26] developed a new variant of the hydrodynamic approach. An important difference of this new variant compared to the model of Benilov is to assume a plasma in chemical non-equilibrium. This new variant was mainly applied to HID lamps. The comparison to the experimental temperature measurements in the thermal plasma showed that the calculated temperature is overestimated by about 4000 K at the mid-plane of the arc [3]. The model developed by Baeva was compared to the model developed by Benilov [4]. It was concluded that the results of the two models are relatively close to each other. The reasons for the differences were difficult to analyze by the authors since both models had to be adapted (as further discussed in [3]) to fulfill implementation constraints imposed by the numerical platforms. The cathode layer model developed by Baeva was also compared to the model developed by Cayla [26]. The former was combined with an arc in partial thermal and chemical equilibrium and the latter with an arc in local thermal equilibrium. The calculated temperatures were compared in the mid-plane of the arc. The results showed that in the central part of the arc, where thermal equilibrium is satisfied, the plasma temperature calculated with the model of Cayla, which is about 13500 K, is about 1500K larger than the temperature calculated with the model of Baeva. Considering the comparisons described above one can conclude that the discrepancies among the models by Benilov, Baeva and Cayla are smaller than the discrepancies of the calculated plasma temperature with the experimental measurement. Baeva et al. [4] also showed that by restricting the arc attachment, a plasma temperature in good agreement with the experimental measurement can be produced. This restriction was however artificially imposed as it was not the result of the physics included in the model. It implies that the physical assumptions made by these models might be inappropriate or some physical phenomena of importance for controlling the arc attachment might be missing.

1.4 Thesis objectives

This thesis work aims to develop a self-consistent model of high-intensity electric arc which can predict GTA in good agreement with available experimental measurements. When the thesis work started, a simulation model for thermal plasma arc in local thermal equilibrium, implemented in an open source CFD software, OpenFOAM®, was available in the Welding Group at University West. This model was not predictive. It required setting boundary conditions on the cathode surface. The present thesis objectives are:

- To understand in details the existing cathode layer models and their underlying assumptions and also to select a suited self-consistent model which is based on physical principles.
- To implement the cathode layer model in a computational software without reformulating the physics to adjust to implementation constraints (usually imposed due to limited access to the source code). This objective is important for being able to analyse the calculation results.
- To test this model independently of the cathode and the thermal plasma arc.
- To develop the coupling between the cathode and the thermal plasma arc through the cathode layer. This is to be done locally along the interface boundary in a way so that the coupling conditions can be updated as often as the systems of equations governing cathode and thermal plasma arc (synchronized coupling). It implies making a suited choice of input parameters for performing the coupling.
- To check the validity of the modelling assumptions that can be questioned, and modify them if needed.
- To apply the coupled model to gas tungsten arc test cases (as used in welding) that have been investigated experimentally in order to verify the calculation results.

1.5 Methodology

To achieve the objective of this thesis a bibliographic study (paper I) was done on cathode layer modelling of thermal arc discharges at atmospheric pressure. The purpose was to give an understanding of the fundamentals

of the cathode layer and also to study the state of the art of its modelling. The main approaches used for modelling the cathode layer were categorized into the diffusion, the partial-LTE and the hydrodynamic approach. The strength and the weakness of each approach were addressed. As described in Section 1.3, the partial-LTE approach is more representative of the physics taking place in the cathode layer than the diffusion approach. It is also more compatible with the objectives of local and synchronized solution of the cathode layer compared to the hydrodynamic approach by Benilov [8]. Therefore, the partial-LTE approach developed by Cayla [12] was chosen for the cathode layer model of the present work.

The cathode layer model was implemented proceeding in several steps. The first implementation step was done in MATLAB using numerical tools provided by this software for solving the systems of equations [34]. MATLAB offers a calculation platform to test the model while avoiding the more sophisticated object-oriented programming which is the main concept in the computational fluid dynamics platform OpenFOAM®. The second step was then to implement the model in OpenFOAM®. It required also implementing the numerical methods needed for carrying out the calculations. In paper II the model is tested with both implementations calculating a one-dimensional problem and the results are compared to results obtained by Cayla [12]. In paper III one-dimensional test cases are calculated to investigate the validity of a number of modelling assumptions. The third step of the model implementation concerned the coupling of the cathode and the LTE-plasma through the cathode layer. In Paper II the coupled model is applied to a planar cathode geometry. In this case the electric conductive coupling applies to all the planar surface of the cathode end. In paper III the coupling boundary condition is extended to a GTA problem with conical electrode, typical of welding applications. This extension necessitates a dynamic modelling of the arc attachment since only part of the cathode tip is electrically conducting. The GTA test cases were based on the experimental set-up used by Haddad and Farmer [27] for measuring the temperature in the plasma core, and by Haidar and Farmer [29] for measuring the temperature on the cathode surface. A set of GTA cases were calculated to test the validity of modelling assumptions related to cathode surface radiative emission and absorption, the electron emission law, the physical state of the cathode. The latter turned out to be incomplete and unsuitable for GTA applications. Paper IV reports the new model proposed for the cathode physical state, its application and testing by comparison to the experimental results.

Chapter 2

Physics and modelling

A deep understanding of the physics of the cathode and the cathode layer is essential to design and implement a cathode layer model as a boundary condition for coupling plasma and cathode. The main role of the cathode is to emit the electrons. The electron emission distribution depends on the morphology and material properties of the cathode. The physics of the cathode regarding the electron emission is reviewed in Section 2.1, and the cathode emission model is summarized in Section 2.2. The cathode layer involves several non-equilibria including deviation from ionization, charge and thermal equilibrium. These non-equilibria take place over different sub-layers. These sub-layers and their main roles in the cathode layer are summarized in Section 2.3.

2.1 Physics of the cathode

In GTA the cathode is usually made of tungsten. Tungsten is a refractory material which is able to produce a thermal arc without melting. The tungsten is commonly activated with a small quantity of rare earth metal oxide, such as thorium dioxide (ThO_2), because of its good characteristics in arc ignition and stability [51]. These activators have a lower work function (e.g. $\phi_{(ThO_2)} = 2.6$ eV) compared to pure tungsten ($\phi_{(W)} = 4.5$ eV). Therefore, although they usually represent only few percent of the cathode weight, they are responsible for emitting the electrons from the cathode surface. It is common in the literature to model the emitters over the cathode surface with an homogeneous distribution. However, some experimental studies [51, 53] have shown that the microstructure of the cathode is modified due to the high temperature reached during arcing. Rare earth metals have a lower melting point (e.g. $T_{m(ThO_2)} = 3323$ K) compared to pure tungsten ($T_{m(W)} = 3653$ K). In the presence of large

cathode temperature they melt. They cannot be dissolved in tungsten [45] and they diffuse due to the temperature gradients from the lower temperature core to the higher temperature surface. This diffusion of emitters is structure dependent and takes place along the grain boundaries which have a longitudinal shape [51]. It is explained by Sadek et al. [51] that the GTA cathode tip geometry is another reason to have a high concentration area of the emitter at the cathode tip. The tip edge indeed cuts across the longitudinal grain boundaries of the tungsten. This leads the diffusing emitters to reach the surface of the tip along the grain boundaries. The emitters then form a layer at the cathode tip if the surface temperature is below the vaporization temperature of the activators. These phenomena change the distribution of the activators from homogeneous to inhomogeneous and thus the electrode ability to emit electrons.

The main electron emission regimes from a cathode surface can be the thermionic, the thermo-field and the field emission. In the thermionic emission regime the electrons are thermally extracted from the cathode surface. It is the dominant emission regime at high temperature. The thermal energy is provided by the ions present in the cathode layer. Thermo-field emission is thermionic emission enhanced by the electric field induced by the ions present in the cathode layer (more specifically in the sheath). In the field emission regime the dominant source of energy for extracting electrons from the cathode is the cathode surface electric field. Field emission thus occurs at high cathode surface electric field. This last emission process uses to be negligible in high-intensity electric arc applications.

In addition to these emission processes secondary electron emission can also take place. The energy needed for emitting secondary electrons is provided by the ions colliding with the cathode surface and bring to the surface an energy larger than the work function.

2.2 Cathode emission model

The existing models of cathode-arc coupling assume a cathode surface covered with homogeneous emitters. In the present thesis work a non-homogeneous cathode model is introduced. The model focuses on the effect of emitter diffusion on the local cathode surface ability to emit electrons. It does not address the diffusion of the emitters in the tungsten matrix. The proposed non-homogeneous cathode model is thus simplified. This simplification is based on the following assumptions.

- The cathode temperature is assumed to remain below the vaporiza-

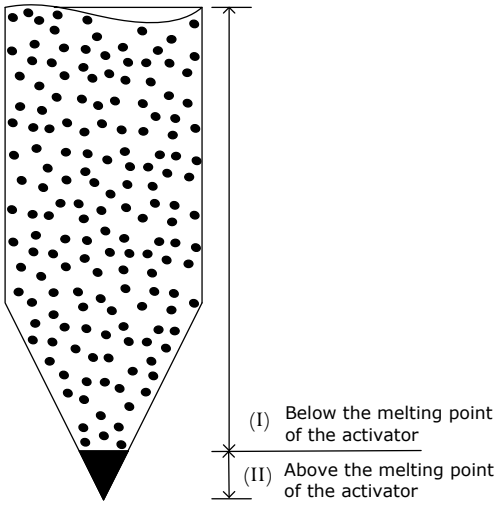

Figure 2.1: Schematic of the activator distribution over the cathode surface during arcing.

tion temperature of the activator.

- The part of the cathode surface where the melting temperature of the activator is reached is assumed to be fully covered by a layer of activator. It means that in this zone, electrons can be emitted from entire part of the cathode surface (physical state (II) in Fig 2.1). The work function for electron emission is related to the activator that covers the surface.

- On the part where the temperature remains lower than the melting temperature of the rare earth oxide, it is assumed that the activators are scattered over the cathode surface. This is similar to the unused electrode. As the activator corresponds only to a few percent of the cathode weight, it can be evaluated that only a few percent of the surface is covered by the activator and thus contributes to the electron emission [59] (physical state (I) in Fig 2.1). The electron emission is thus assumed in this study to be small enough to be neglected.

For refractory cathodes used in GTA the cathode surface temperature is high and the electron emission is commonly calculated with the Richardson-Dushman equation supplemented with Schottky correction. It applies the thermionic emission enhanced by a cathode surface electric field. The validity of this equation in the range of low cathode surface temperature and high cathode surface electric field has been questioned [20, 21, 30]. The Murphy-Good equation is another emission law

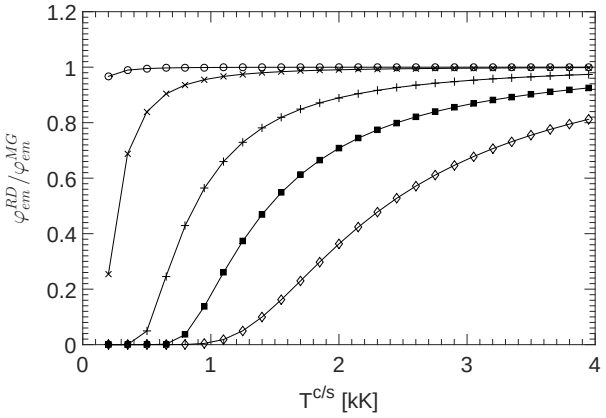

Figure 2.2: Ratio of the Richardsson-Duschmann-Schottky to Murphy-Good emission flux as function of the cathode surface temperature for ThO_2, and a cathode surface electric field of: $(\circ)10^7$, $(\times)10^8$, $(+)5\times10^8$, $(\blacksquare)10^9$ and $(\diamond)2\times10^9$ V/m.

which is characterized by a larger domain of validity. The ratio of current density calculated with the Richardson-Dushman-Schottky model, φ_{em}^{RD}, and the Murphy-Good model, φ_{em}^{MG}, is illustrated in Fig 2.2 with respect to the temperature and the electric field on the cathode surface. As expected, it can be seen that the discrepancy is higher at low cathode surface temperature and the high cathode surface electric field.

2.3 Physics of the cathode layer

This section gives a brief summary of the fundamentals of the cathode layer and its physics. The cathode layer is the place of different non-equilibria associated with characteristic lengths that are defined as follows. The Debye length, λ_D, is the scale over which the ions are screened by the electrons. The smallest mean free path, λ_c, is the distance travelled by a charged particle before colliding with another charged particle. The recombination length, λ_r, is the scale at which the recombination and ionization rate is of the same order as the rate of variation of the electron and ion density due to ambipolar diffusion. The electron energy relaxation length, λ_e, is the length over which the electrons dissipate the energy they gain from the electric field while colliding with heavy particles. These characteristic length were evaluated for an argon plasma and can be ordered as $\lambda_D \ll \lambda_c \ll \lambda_r \ll \lambda_e$ [8]. This ordering implies that the cathode layer can be decomposed into sub-layers characterized by distinct dominant physics. The main properties of these sub-layers are

now summarized.

2.3.1 Sheath (space charge layer)

The first sub-layer on the cathode surface is the sheath (or the space charge layer) and it has a thickness of the order of λ_D. It implies that the local charge neutrality is not satisfied in this region. As can be seen in Fig 2.3, it mainly consists of positive ions attracted by the negative charge of the cathode surface. A potential barrier is consequently formed in the vicinity of the cathode. This region is also almost collisionless and thus modelled with collisionless kinetic theory. The thermodynamic equilibrium therefore cannot be defined. The main roles of the cathode sheath are:

- To enhance the cathode surface electron emission by lowering the cathode surface potential barrier.
- To accelerate the emitted electrons and provide them with sufficient kinetic energy to promote impact ionization in the pre-sheath layer.
- To accelerate the ions generated in the pre-sheath towards the cathode surface. The kinetic energy transferred by the ions increases the cathode surface temperature and thus contributes to the thermionic electron emission. Some of the ions with high kinetic energy may also promote secondary electron emission.
- To reduce the number of back diffusion electrons from the pre-sheath towards the cathode.

2.3.2 Knudsen layer

The second sub-layer from the cathode surface is the Knudsen layer and it has a thickness of the order of λ_c. This sub-layer is also dominated by the electric field acceleration. However, contrary to the sheath it is locally neutral and collisional, although the collision frequency is not sufficient to reach the local thermal equilibrium. Its main role is to accelerate the ions up to the Bohm velocity. The Bohm velocity represents the minimum ion velocity allowing forming the sheath.

2.3.3 Pre-sheath (ionization layer)

The pre-sheath is the region where charged species are produced by ionization. As in this study the pressure is of the order of the atmospheric

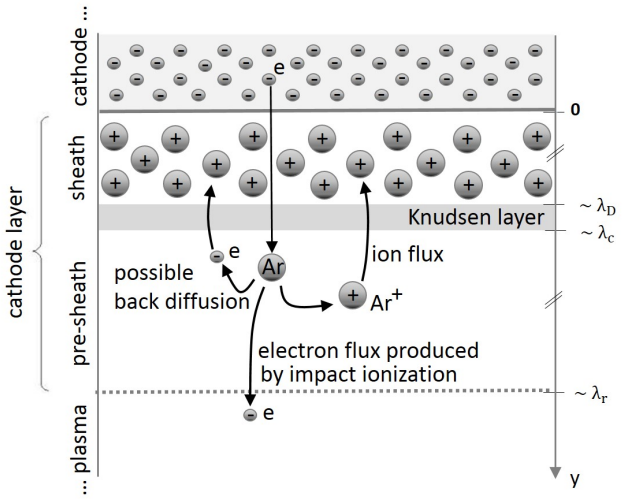

Figure 2.3: Sketch of the sub-layers of the cathode layer in GTA (no scale).

pressure, the dominant ionization process is the impact ionization. As can be seen in Fig 2.3, the impact ionization takes place when an electron emitted from the cathode surface and sufficiently accelerated in the sheath impacts with an atom or an ion in the pre-sheath. The ions provided by the ionization move towards the cathode. The electrons provided by the ionization go towards the plasma. Some electrons, called the back diffusion electrons, though might have enough energy to go through the sheath and reach the cathode. The pre-sheath has a thickness of the order of λ_r. Thus local ionization-equilibrium is not satisfied in this layer. The thermal equilibrium is partial in which the electron temperature is larger than heavy particle temperature.

2.4 Main cathode layer modelling assumptions

The cathode layer model of short high-intensity arc used in this work is based on the following main assumptions.
For the sheath:

- The emitted electrons are at thermal equilibrium with the cathode surface.
- The space charge of emitted electrons is neglected when calculating the cathode surface electric field [10].
- The cathode sheath is collisionless.

- The temperature of the back diffusion electrons is constant along the sheath and is equal to the electron temperature at the sheath/pre-sheath interface.
- The nearly isotropic distribution functions of the back diffusion electrons in the sheath can be approximated by a Maxwellian.
- All the ions reaching the cathode surface are recombined.

For the Knudsen layer:

- The ions leave the Knudsen layer and enter the sheath with the Bohm velocity [50].
- In the Knudsen layer, the component normal to the cathode wall of the ion distribution function can be approximated by an Heaviside distribution function defined based on Bohm velocity.

And for the pre-sheath layer:

- Real gas effect can be neglected in the pre-sheath since it is at pressure of the order of atmospheric pressure.
- Radiative ionization is negligible.
- The ionization energy is provided by the impacting electrons.
- The pre-sheath is assumed to be in static equilibrium.

2.5 System of equations

The details of the cathode layer model derivation are reported in Appendix A. The main outputs of the model are the sheath voltage drop, U^s, the net heat flux to the cathode surface, $q^{cl\rightarrow c}$, and the electron temperature at the sheath/pre-sheath interface, $T_e^{s/ps}$. They are obtained by solving two sets of non-linear equations. The first one is to provide the number densities of the plasma components at the sheath/pre-sheath ($n_e^{s/ps}, n_{Ar^+}^{s/ps}, n_{Ar^{2+}}^{s/ps}, n_{Ar^{3+}}^{s/ps}$) and at the pre-sheath/plasma ($n_e^{p/ps}, n_{Ar^+}^{p/ps}, n_{Ar^{2+}}^{p/ps}, n_{Ar^{3+}}^{p/ps}$) interfaces, as illustrated in Fig 2.4. This system of equations includes the detailed balance through Saha law (eq. A-1), the Dalton's law of partial pressures (eq. A-5) and the electric neutrality (eq. A-6).

Knowing the plasma compositions, the ion flux, φ_i (eq. A-7), the back diffusion flux, φ_{bd} (eq. A-11), the thermo-field emission flux, φ_{em} (eq.

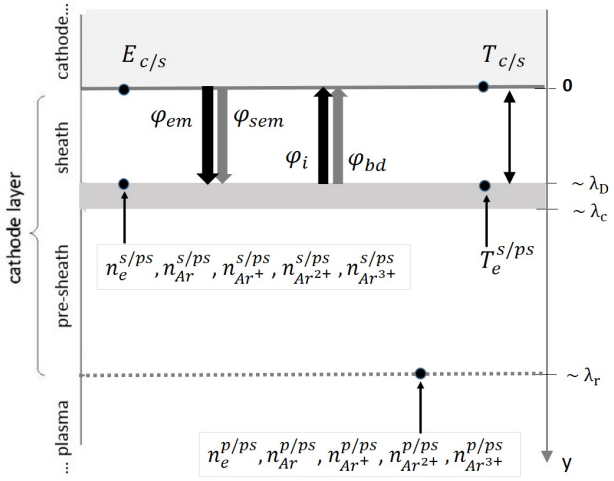

Figure 2.4: Sketch of the cathode layer structure with key variables (no scale).

A-14) and the secondary emission flux, φ_{sem} (eq. A-13), are determined. These fluxes and the plasma components are then used to form the second set of non-linear equations. This system of equations includes the current conservation at the cathode surface (eq. A-28), the energy balance at the cathode surface (eq. A-29 and eq. A-44) and the energy balance in the pre-sheath (eq. A-53). By solving this second set of equations the outputs of the model are obtained. The numerical procedure of the calculation is presented in Chapter 3.

Chapter 3

Numerical procedures

The cathode model, the plasma model and the cathode layer model at their interface are implemented in OpenFOAM®, which is an open source software based on C++ classes and libraries used mostly for computational fluid dynamics. The coupling is performed locally for each element at the cathode-plasma interface. The main input to the cathode layer model is the current density at the cathode surface (or at the cathode/sheath interface), $j^{c/s}$, which is provided by the cathode model. Additional quantities are also collected from the cathode and the plasma cells adjacent to the interface. These quantities are the local cathode temperature, T^c, its corresponding thermal conductivity, $\kappa^c(T^c)$, and the boundary-normal width of the boundary cell at the cathode, δ^c, the pressure, P and the plasma temperature T^p. The outputs are the sheath voltage drop, U^s, the net heat flux to the cathode surface, $q^{cl\rightarrow c}$, and the electron temperature at the sheath/pre-sheath interface, $T_e^{s/ps}$. The two latter are used to set the coupling boundary condition. $q^{cl\rightarrow c}$ is used to set the energy boundary condition for the cathode region at the interface. $T_e^{s/ps}$ is used to set electric potential boundary condition for the cathode and the plasma region and the energy boundary condition for the plasma region. The numerical procedure is presented in two steps. The first step concerns the local numerical procedure for solving the system of equations inside the cathode layer. The second step addresses the global numerical procedure for the complete calculation including the cathode and the plasma, coupled through the cathode layer.

3.1 Local numerical procedure

As can be seen in Fig 3.1, the local numerical procedure of the cathode layer model is an iterative method. It starts by using the initial values

of the unknowns, $(U^s)_0$, $(T_e^{s/ps})_0$ and $(T_h^{s/ps})_0$. These initial values are provided to the cathode layer model from the previous global iteration. The additional quantities needed to solve the equations are also collected from the cathode and the plasma region. The number densities of the plasma components are then calculated using the first set of equations described in Section 2.5 and provided in Appendix A. This system of five non-linear equations is solved according to the calculation method proposed by Godin [25]. This method is based on the concept of the chemical basis, which is a subset of species from which all other species may be formed by means of chemical reactions. After obtaining the number densities of the plasma components the main fluxes of charged particles through the sheath are calculated. These fluxes are used in the energy and charge conservation equations which form the second set of equations mentioned in Section 2.5 and provided in Appendix A. This second set of equations is highly non-linear and produces a complex Jacobian matrix that is difficult and expensive to calculate. Therefore, this second system is solved with the Secant method, which is basically the Newton-Raphson algorithm but approximating the Jacobian matrix through finite differences. The converged cathode layer model provides the data needed for the coupling boundary condition used in the global numerical procedure.

3.2 Global numerical procedure

Considering the global numerical procedure including the cathode and the plasma, the main steps of each global iteration are given as follows. In the cathode

1. Solve the energy equation (A-54).
2. Update the temperature dependent properties, σ^c, κ^c.
3. Solve the electric potential equation (A-58).
4. Solve the magnetic potential equations (A-59).
5. Update the electric field, $\mathbf{E}$, and the current density, $\mathbf{j}$.

In the thermal plasma

6. Solve the system of Navier-Stokes equations (A-55)-(A-56).
7. Solve the energy equation (A-57).

8. Calculate the temperature from the enthalpy and update the temperature dependent thermodynamic and transport properties, including ρ, and σ^p.
9. Solve the electric potential equation (A-58).
10. Solve the magnetic potential equations (A-59).
11. Update the electric field, **E**, the current density, **j**, and the magnetic field **B**.

The cathode layer model is employed each time the energy and electric potential boundary conditions are needed. It means that in steps 1, 3, 7 and 9 of the global calculation the local numerical procedure is applied.

3.3 Dynamic arc attachment

In GTA applications the cathode/plasma interface is not everywhere electrically conductive along the conical cathode tip. Therefore the coupling needs to be applied differently on different parts of the interface. The part of the interface where the thermal plasma arc is not attached (electrically non-conductive) then needs to be distinguished from the part where the arc is attached (electrically conductive). Based on the cathode physics described in Section 2.2, the melting temperature of the activator is used as a criterion to determine the arc attachment and the activation/deactivation of the cathode layer model. At each global iteration this criterion is locally checked for each discrete element of the cathode surface. If the temperature, T^c, of an element is larger than the criterion, the cathode is in the physical state (II), in which the arc attachment is enabled and the cathode layer model is activated. If T^c is smaller than the criterion, the cathode is in the physical state (I) which is not favourable to arc attachment and the cathode layer model is deactivated. This leads to a dynamic arc attachment and two types of coupling boundary conditions, i.e. with and without arc attachment.

3.3.1 Surface element without arc attachment

The surface elements outside the arc attachment are assumed to be electrically non-conductive. The electric potential boundary condition is thus applied accordingly (see Tables 3.1 and 3.2). It is known that the LTE plasma assumption leads to an overestimation of the plasma temperature in the colder plasma region [3]. This overestimation causes an overestimation of the cathode temperature when using the thermal conducting

	with arc attachment	without arc attachment
T	(3.2)	$\partial_n T = 0$
V	(3.3) with (3.4)	$\partial_n V = 0$

Table 3.1: Boundary conditions at the cathode-plasma interface for the plasma region.

	with arc attachment	without arc attachment
T	(3.1)	$\partial_n T = 0$
V	(3.3) with (3.5)	$\partial_n V = 0$

Table 3.2: Boundary conditions at the cathode-plasma interface for the cathode region.

coupling boundary condition. Therefore, a thermally insulated coupling boundary condition is assumed for the surface elements outside the arc attachment.

3.3.2 Surface element with arc attachment

For the surface elements inside the arc attachment the cathode layer model is applied locally and solved according to the numerical procedure summarized in the flowchart in Fig. 3.1. The outputs $T_e^{s/ps}$, $T_h^{s/ps}$, and $q^{cl\to c}$ are used to set the interface boundary conditions for both the cathode and the plasma. On the cathode surface elements the temperature gradient normal to the boundary is fixed based on the heat flux from the cathode layer as,

$$\partial_n T^c = \frac{q^{cl\to c}}{\kappa^c}. \tag{3.1}$$

On the plasma surface elements the boundary surface temperature, $T^{p/cl}$, is set with the help of $T_h^{s/ps}$ and $T_e^{s/ps}$ as [9],

$$T^{p/cl} = \begin{cases} T_h^{s/ps} & \text{if } \kappa^p(T_h^{s/ps}) \gg \kappa^p(T_e^{s/ps}) \\ T_e^{s/ps} & \text{if } \kappa^p(T_e^{s/ps}) \gg \kappa^p(T_h^{s/ps}) \\ \frac{1}{2}\left(T_e^{s/ps} + T_h^{s/ps}\right) & \text{otherwise} \end{cases} \tag{3.2}$$

The electric potential boundary conditions on the cathode, $V^{c/cl}$, and on the plasma, $V^{p/cl}$, face elements are set based on the current density

conservation as,

$$V^{p/cl} = V^{c/cl} = \frac{V^c \sigma^c \, \delta^p + V^p \sigma^p \, \delta^c}{\sigma^c \, \delta^p + \sigma^p \, \delta^c}, \tag{3.3}$$

where the electrical conductivities are $\sigma^c = \sigma^c(T^c)$ and $\sigma^p = \sigma^p(T_e^{s/ps})$. To avoid large oscillations when solving the electric potential the coupling boundary condition is applied as a mixed boundary condition. The mixed boundary condition is a combination of the Dirichlet and the inhomogeneous Neumann condition. It is controlled by the bounded value fraction α ($0 \leq \alpha \leq 1$), defined by

$$\alpha = \alpha^p = \frac{\sigma^c \, \delta^p}{\sigma^p \, \delta^c + \sigma^c \, \delta^p}, \tag{3.4}$$

for the plasma boundary condition, and

$$\alpha = \alpha^c = \frac{\sigma^p \, \delta^c}{\sigma^c \, \delta^p + \sigma^p \, \delta^c}, \tag{3.5}$$

for the cathode boundary condition. This method preserves the current density conservation and provides more stability of the electric potential solution.

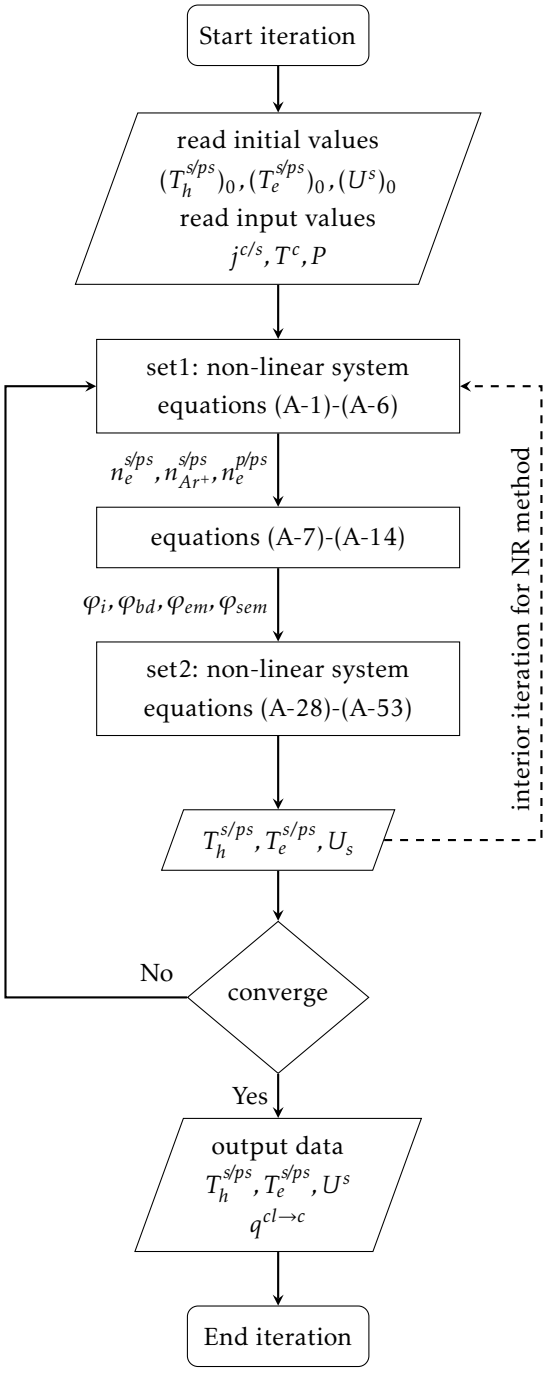

Figure 3.1: The cathode layer model calculation flowchart

Chapter 4

Summary of the results

The main calculation results of this work can be summarized in three parts. The first part examines the results obtained with the cathode layer model without the coupling to the cathode nor the plasma (Section 4.1). The second part investigates the validity of different modelling assumptions concerning the cathode layer and the cathode (Section 4.2). The third part compares with experimental measurements the results obtained when coupling the cathode and the plasma through the cathode layer (Section 4.3).

The test cases calculated for the cathode layer model alone are one-dimensional. The cathode and the plasma are then reduced to boundary conditions. The plasma is argon gas at atmospheric pressure. The cathode is 1 cm high and water cooled at 1000 K. It is made of pure tungsten (for comparisons with results obtained by Cayla) and thoriated tungsten (as in GTA welding). The range of current density studied, which includes the GTA range, goes from 10^4 to $5{\times}10^8$ $A.m^{-2}$. The test cases with cathode and plasma coupled through the cathode layer are set based on experimental studies of GTA [27, 28]. The cathode material is thoriated tungsten, the arc length is 5 mm, and the shielding gas is argon at atmospheric pressure. The water cooled copper anode is not included in the calculation domain and is reduced to a boundary condition. The GTA cases presented in this chapter are at 200 A.

4.1 Cathode layer model results

The main results provided by the cathode layer model are summarized in this section. Figs 4.1 and 4.2 represent respectively the argon and electron number densities at the sheath/pre-sheath (non-LTE) and at the plasma/pre-sheath (LTE) interfaces against the current density at the

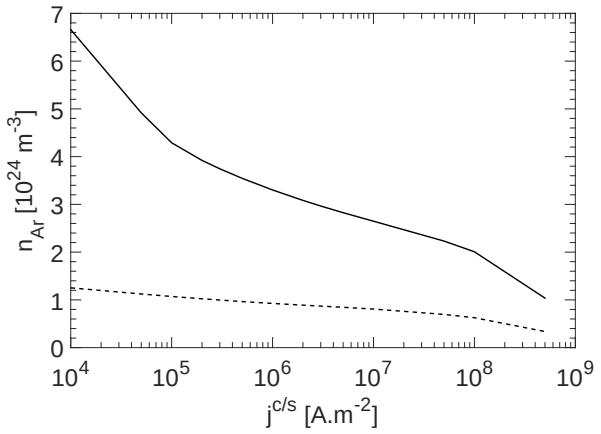

Figure 4.1: Argon number density at the LTE plasma/pre-sheath interface (dashed line) and the non-LTE sheath/pre-sheath interface (solid line) as a function of the current density at the thoriated tungsten cathode surface.

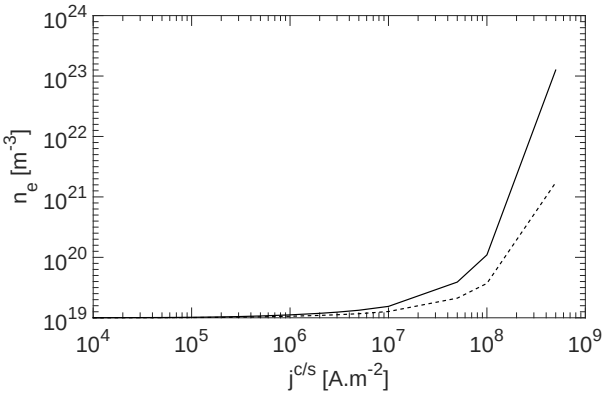

Figure 4.2: Electron number density in LTE plasma/pre-sheath interface (dashed line) and the non-LTE sheath/pre-sheath interface (solid line) as a function of the current density at the thoriated tungsten cathode surface.

tungsten cathode surface. The calculation results show the significant effect of the thermal non-equilibria characteristic of the pre-sheath on the number densities. The ion number densities are also derived from the argon and electron chemical basis (see Godin's calculation method in Chapter 3) leading to the pre-sheath composition. Fig 4.3 illustrates the pre-sheath composition at the plasma interface (which is in LTE). One can see that by increasing the cathode surface current density the number of argon ions increases. The dominant ion specie in the pre-sheath is the ion Ar^+. Ar^{2+} starts to be present when the current density $j^{c/s}$ goes beyond

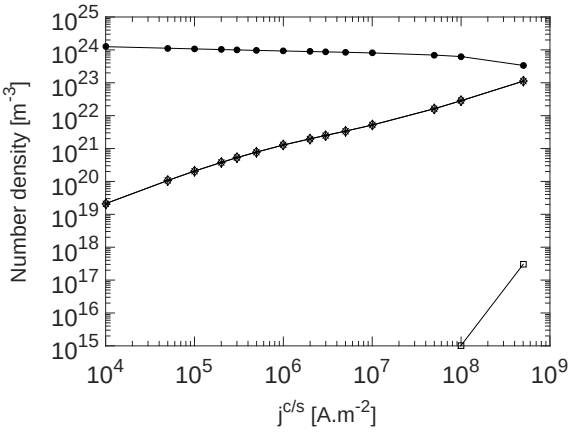

Figure 4.3: Plasma composition for an LTE plasma at atmospheric pressure the current density at the cathode surface. (◇) ne, (●) nAr, (★) nAr^{+}, (□) nAr^{2+}.

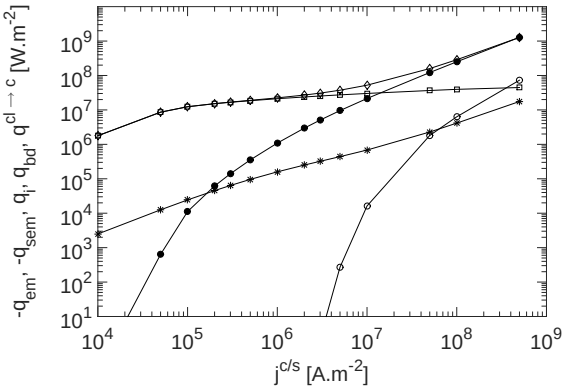

Figure 4.4: Heat flux components of thoriated tungsten cathode as functions of the current density at the cathode surface. (◇) q_i, (●) q_{em}, (★) q_{sem}, (○) q_{bd}, (□) $q^{cl\to c}$.

10^8 A/m^2. Ar^{3+} is not observed within the pre-sheath in the range of current density studied.

Fig 4.4 shows the heat fluxes to the cathode. It can be seen that the ion heat flux is always the leading heating process. It is almost equal to the net heat flux, up to $10^6 A.m^{-2}$ of the current density. It can be observed that the contribution of the secondary emission heat flux to the net heat flux is significant for a cathode current density less than $5\times10^5 A.m^{-2}$. One can also see that for a cathode current density higher than $2\times10^5 A.m^{-2}$, the net heat flux remains constant at about $2\times10^7 W.m^{-2}$. This is due to the high cooling effect of the emitted electrons. This constant heat flux to the cathode causes a linear increase in cathode temperature (see Fig (4.7) for

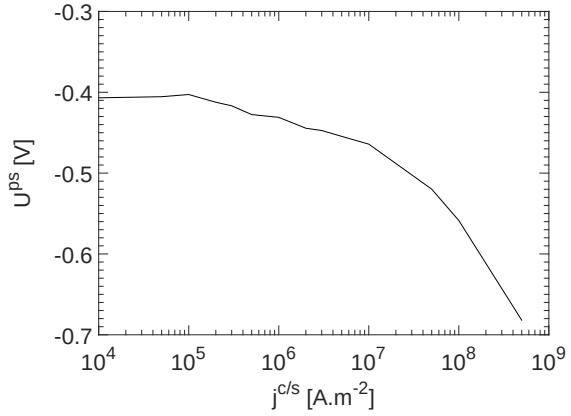

Figure 4.5: Pre-sheath voltage drop as functions of the current density at the thoriated tungsten cathode surface.

thoriated tungsten).

Fig 4.5 shows the voltage drop in the pre-sheath, U^{ps}, as function of the current density at the thoriated tungsten cathode surface. It results from the gradient in charge density through the pre-sheath. It is more than one order of magnitude smaller than the voltage generally measured in GTA.

Figs 4.6 and 4.7 show the comparison of the calculation results, namely sheath voltage drop and cathode surface temperature, with the results obtained by Cayla [12] for a tungsten cathode. The results obtained using a thoriated tungsten cathode are also presented in those figures. As can be seen a good agreement with the results by Cayla is obtained. It can be seen in Fig 4.6 that U^s is almost constant and at a minimum value of the order of 8 eV when $j^{c/s} \geq 10^7 W.m^{-2}$. This minimum sheath voltage drop is of the same order of magnitude as the voltage generally measured in GTA. It thus confirms that the sheath voltage drop is not negligible. In this range the cathode surface temperature, $T^{c/s}$, is large enough to promote termoionic emission. When going down towards lower values of $j^{c/s}$, the sheath potential, U^s, increases to compensate with field enhanced emission the lower thermoionic emission. The cathode surface temperature $T^{c/s}$ as a function of the cathode surface current density $j^{c/s}$ is showed in Fig 4.7. For tungsten and $j^{c/s}$ between 10^4 and $10^6 A.m^{-2}$, where the transition from dominant seconday emission to field-enhanced thermoionic emission and then thermoionic emission successively take place, $T^{c/s}$ increases significantly and non-linearly. At larger values of $j^{c/s}$ thermoionic emission is established, the cathode net heat flux $q^{cl \to c}$ is constant, and $T^{c/s}$ increases linearly. It is also observed that the thoriated tungsten leads to a significantly lower cathode surface temperature, as

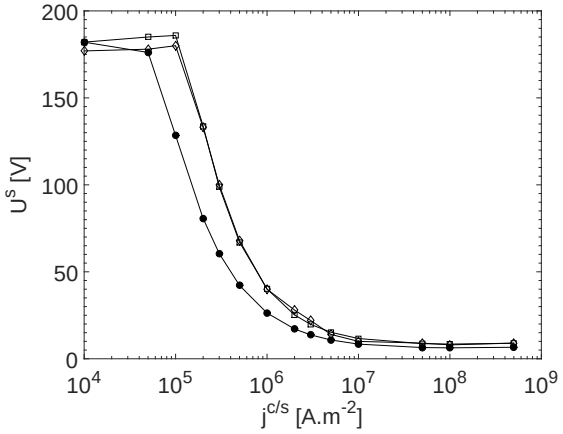

Figure 4.6: Sheath voltage drop as functions of the current density at the cathode surface. (●) thoriated tungsten, (□) tungsten and (◇) tungsten by Cayla [12].

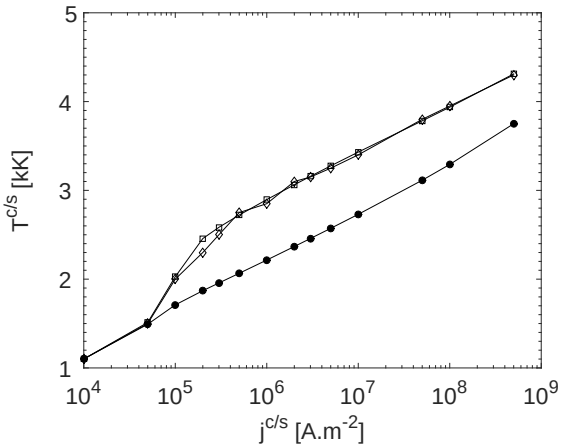

Figure 4.7: Cathode surface temperature as functions of the current density at the cathode surface. (●) thoriated tungsten, (□) tungsten and (◇) tungsten by Cayla [12].

well as a lower sheath potential, compared to pure tungsten. This is an expected consequence of its lower work function.

4.2 Verification of assumptions

The verification of different modelling assumptions, some of them being also questioned in the literature, is presented in this section.

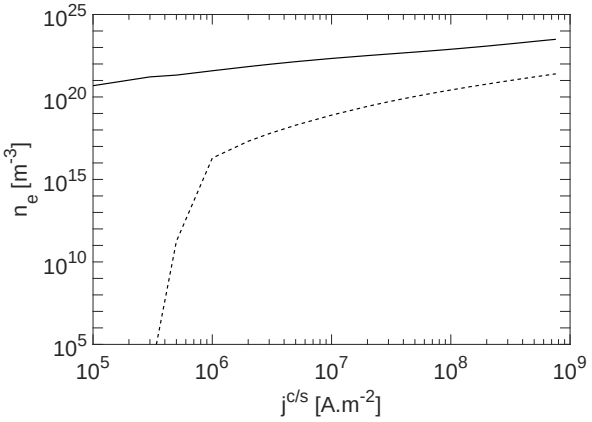

Figure 4.8: Sheath electron number density (solid line) and cathode surface emitted electron number density (dashed line) as a function of the current density at the cathode surface.

The space charge of emitted electrons

Fig 4.8 compares the sheath total electron number density and the emitted electron number density from the cathode surface as a function of the cathode surface current density. It shows that the number of emitted electrons does not exceed 1% of the number of electrons in the sheath. The assumption of negligible number of emitted electrons inside the sheath [7] which is done when calculating the cathode surface electric field is thus confirmed to be valid for the applications of this study.

Secondary electron emission

As illustrated in Fig 4.4, the secondary electron emission is not a negligible emission process at low current density. Such low current density might be met for HID lamps. However, Fig 4.11 shows that for the gas tungsten arc applications investigated in this study, the heat flux due to secondary electron emission is negligible compared to the heat flux transported by ions and emitted electrons.

The emission law

The validity of the Richardson-Dushman emission law was questioned for low work function materials [20]. The rare earth metals used for doping tungsten electrodes of GTA applications are characterized by a low work function. The validity of the Richardson-Dushman law was thus investigated. Figs 4.9 illustrates the electric field strength on the cathode surface calculated with the cathode layer model. Considering

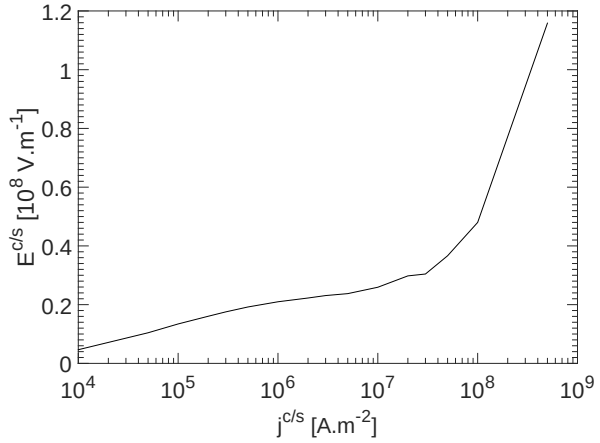

Figure 4.9: Electric field strength at the cathode surface as a function of the current density at the cathode surface.

the range of electric field and of cathode surface temperature (see Fig 4.7 for thoriated tungsten) and referring to Fig 2.2, one can see that the Richardson-Dushman emission law is used in its domain of validity, since $\varphi_{em}^{RD}/\varphi_{em}^{MG} = 1$. It is thus justified to use the Richardson-Dushman emission law supplemented with Schottky correction for modelling the rare earth electron emitters used in GTA welding. This law is numerically simpler to calculate than the Murphy-Good law. It was observed by this study that the computational cost of the Richardson-Dushman law can be up to 50 times lower than the Murphy-Good law.

The radiative model

The effect of the cathode surface heating and cooling by radiative absorption, q_{rad}^{abs}, and emission, q_{rad}^{em}, are illustrated in Figs 4.10 and 4.11. Fig 4.10 shows that the cathode surface heating by radiative absorption is at the same order of magnitude as the cathode surface cooling by radiative emission. One can conclude that the cathode surface radiative absorption is not negligible compared to radiative emission. Fig 4.11 compares the radiative heat fluxes with other cathode surface heat fluxes. It is observed that at the cathode tip q_{rad}^{abs} and q_{rad}^{em} contribute to less than 1% of the heating and cooling energy fluxes of the cathode surface.

The cathode model

In GTA applications the physical state of the cathode uses to be assumed homogeneous which is in contradiction with the cathode inhomogeneity observed experimentally. The effect of the non-homogeneous distribution

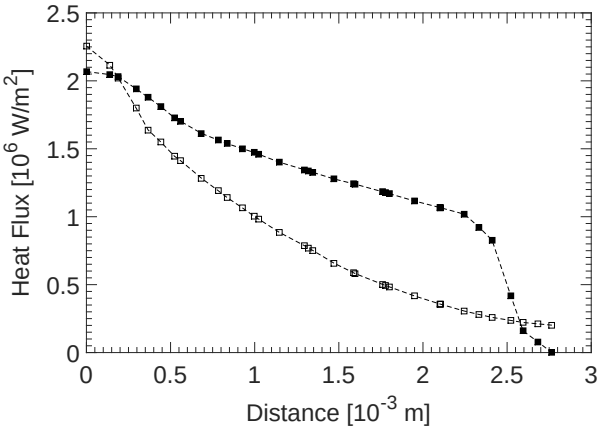

Figure 4.10: Radiation heat fluxes along the cathode surface as functions of the distance from the tip center, 200 A. (□, ■) absorbed and emitted heat flux (q_{rad}^{abs}, q_{rad}^{em}).

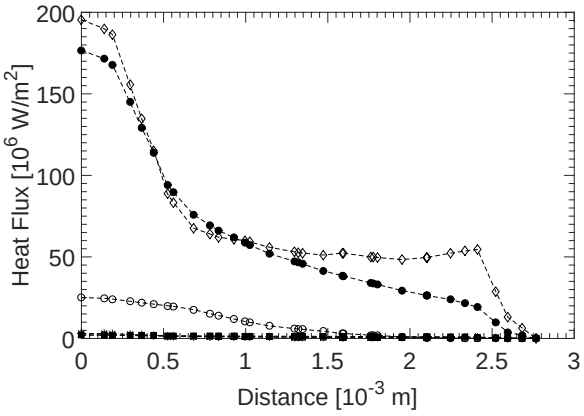

Figure 4.11: Heat flux components along the cathode surface as function of the distance from the tip center, 200 A. (◇) q_i, (●) q_{em}, (★) q_{sem}, (○) q_{bd}, (□) q_{rad}^{abs}, and (■) q_{rad}^{em}.

of the cathode emitters on the size of the arc attachment was thus investigated. It is observed in Fig 4.12 that when using an homogeneous cathode model (physical state (II)) the arc attachment covers almost the entire length of the cathode tip (about 90% of the tip length fraction at 200 A). The proposed non-homogeneous model leads to a smaller arc attachment (about 23% of the tip length fraction at 200 A). Available pictures of experimental observations during arcing [51, 54] report an arc attachment spot covering about 25% of the tip length fraction for a current intensity of 200 A. The arc attachment length predicted by the non-homogeneous cathode

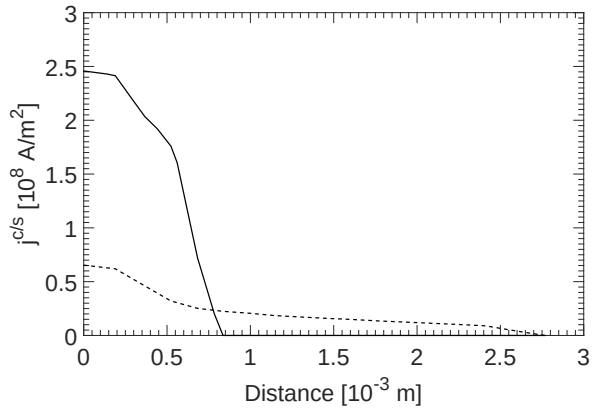

Figure 4.12: Surface-normal current density along the cathode surface as functions of the distance from the tip center, 200A. (⋯, —) calculation results of the (homogeneous, non-homogeneous).

model is thus much closer to the experimental observations than when calculated with the homogeneous model. However, these comparisons are only quantitative since the exact extent of the cathode arc spot was not measured experimentally. The arc attachment is known to govern the temperature distribution on the cathode surface and within the plasma column. These quantities are accessible to experimental measurement and can be used to test the model.

4.3 Comparison to temperature measurements

Fig 4.13 shows the comparison of the cathode surface temperature experimentally measured by Haidar and Farmer [29] for a GTA configuration with a water cooled anode and the numerical results calculated with the homogeneous and non-homogeneous cathode model. It can be clearly seen that the non-homogeneous cathode model predicts the cathode surface temperature closer to the experimental measurement than the homogeneous model.

Figs 4.14 and 4.15 compare the plasma temperature with the experimental observation by Haddad and Farmer [27] for the same GTA configuration. In Fig 4.14 the plasma temperature calculated, using the two cathode models, is compared with the experimental measurement along the arc axis. A similar comparison is made in Fig 4.15 but along the radial direction at various distances below the cathode tip. Both figures reveal the significant effect of using a non-homogeneous cathode model on the plasma temperature. A good agreement is observed between the

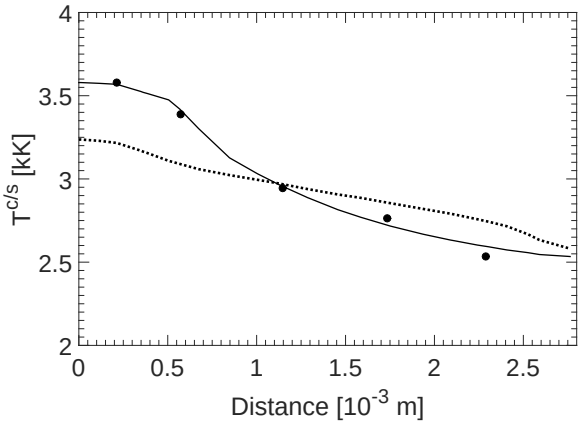

Figure 4.13: Temperature along the cathode surface as functions of the distance from the tip center, 200A. (•) experimental results of Haidar and Farmer [29] and (···, —) calculation results of the (homogeneous, non-homogeneous).

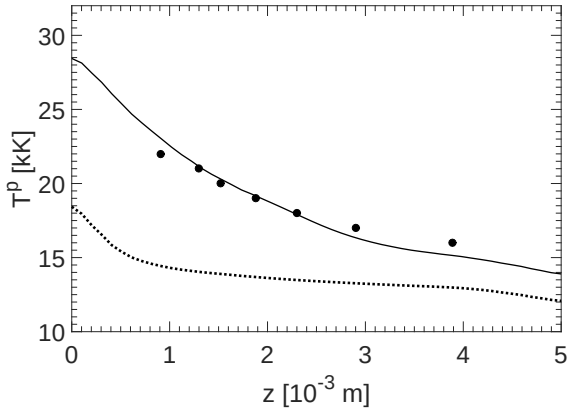

Figure 4.14: Plasma temperature along the symmetry axis as functions of the distance from the tip center, 200A. (•) experimental results of Haddad and Farmer [27] and (···, —) calculation results of the (homogeneous, non-homogeneous).

non-homogeneous model and the experimental results. Small discrepancies are however observed in Fig 4.15 when the plasma temperature goes below about 12000 K. They can be explained by the fact that the local thermal equilibrium assumption cannot properly describe the plasma in cold regions.

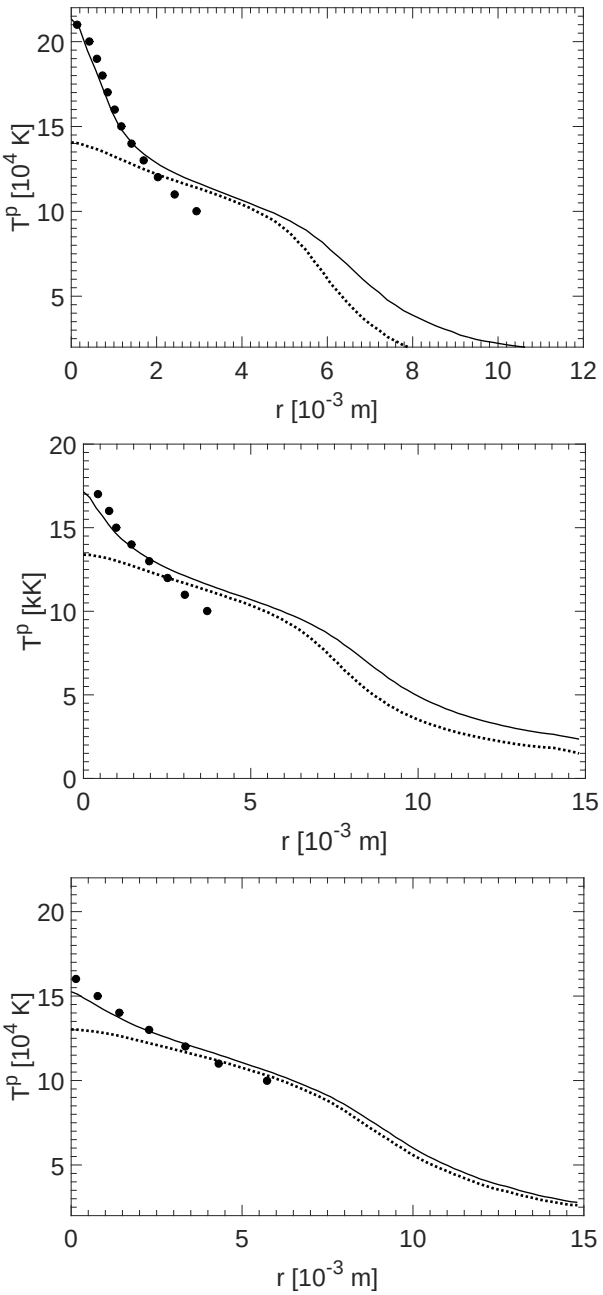

Figure 4.15: Plasma temperature along the radial direction, r. Top: z=1.25 *mm*, Center: z=2.5 *mm*, and Bottom: z= 3.75 *mm* from the cathode tip, 200*A*. (•) experimental results of Haddad and Farmer [27] and (⋯, —) calculation results of the (homogeneous, non-homogeneous).

Chapter 5

Concluding remarks

The main goal of the present thesis work was to develop a self-consistent model of high-intensity electric arc for predicting gas tungsten arc as used in welding. In response to this, a survey on different cathode layer models was done. The main modelling approaches were categorized into the diffusion approach, the partial-LTE approach and the hydrodynamic approach (Paper II). It was found that the partial-LTE approach (with the model of Cayla [12]) is more compatible with the objectives of local and synchronized numerical solution of the cathode layer model compared to the hydrodynamic approach (the comprehensive model of Benilov [10]).

The cathode layer model by Cayla [12] was thus investigated and implemented proceeding in successive steps, first in MATLAB [34] and then in OpenFOAM® (Paper II and Paper III). An important constraint fixed for the numerical implementation was to avoid reformulating the model (i.e. modifying the physics) for numerical convenience. This type of numerical adaptation would indeed make it difficult to interpret the calculation results. The cathode layer model was successfully tested by comparison to calculation results obtained by Cayla [12] for a one-dimensional test case. It was coupled with an LTE-plasma model and with a cathode model. The coupling was developed in successive steps. In the first step it was applied to a test case with planar cathode geometry (Paper I), and next to a GTA problem that had been investigated experimentally [27, 29] (Paper III and Paper IV).

In the present thesis work the validity of different modelling assumptions, some being questioned in the literature, was assessed. These investigations can be summarized as follows:

– It was verified that it is valid to neglect the space charge of emitted electrons when calculating the cathode surface electric field (Paper III).

- While it was known that the secondary electron emission cannot be neglected in low current density HID lamps [12], it was found that for gas tungsten arc applications its effect is negligible compared to the effect of other energy fluxes (Paper III).

- Using the Murphy-Good emission law as a reference, it was verified that the Richardson-Dushman emission law supplemented with Schottky correction is used in its domain of validity when applied to a low work function rare earth oxide used for doping gas tungsten arc cathodes (Paper III).

- It was observed that the cathode surface radiative absorption cannot be considered negligible compared to the radiative emission. It was also observed that both emission and absorption radiative fluxes are negligible compared to the other energy fluxes at the end tip of a GTA the cathode surface (Paper IV).

- It was observed that the usual assumption of uniform distribution of the electron emitters on the cathode surface does not allow reproducing the cathode surface temperature and the plasma core temperature measured experimentally. It was found that this assumption of non-uniformity is in contradiction with the literature documenting experimental observations of doped GTA cathode during arcing. The cathode model was extended to a first level of non-uniformity of the distribution of the electron emitters. The calculation results showed that this non-uniformity has a significant effect on the size of the arc attachment, on the cathode surface temperature, and on the plasma core temperature. A much better agreement with the experimental measurements was then obtained (Paper IV).

This work addressed the prediction of the current density distribution along the cathode surface of a GTA arc. A self-consistent model based on physical principles was further developed. Its numerical implementation did not alter the physics of the model, and allows a local and synchronized updating of the cathode and plasma coupling condition. Contrary to the models used so far, the model developed in this study can predict trends observed experimentally without making use of any adjustable numerical parameter.

5.1 Future work

The following improvements and developments could be done.

- The plasma model could be extended to a partial-LTE model. This would help to obtain better results in the area where the LTE assumption is not valid.
- The cathode layer model could then be extended to the electrically non-conducting part of the cathode boundary.
- The influence of charge diffusion in the cathode pre-sheath (included in the cathode layer hydrodynamic approach and neglected in the partial-LTE approach for the pre-sheath) could be investigated.
- The influence of the local thickness of the cathode layer could be investigated. It is known to vary with the cathode surface conditions, and all the models developed up to today assume it uniform.
- The simplified non-homogeneous cathode model proposed in this study could be further developed.
- The cathode layer model could be extended to the anode layer and applied as an anode-plasma coupling boundary to provide the heat flux to the work piece.

Chapter 6

Summary of papers

This chapter provides a short summary of the papers appended at the end of the thesis.

Paper I

A review of cathode-arc coupling modelling in GTAW

Paper I summarizes the latest state of the art of the cathode layer model employed in GTAW at atmospheric pressure. The physics of the cathode layer model was addressed and the details of the sub-layers and the main role of each were discussed. These main sub-layers were distinguished based on the different specific characteristic length recognized in the cathode layer. These sub-layers are the sheath (associated with Debye length), the Knudsen layer (related to smallest mean free path) and the pre-sheath (associated with recombination length).

Based on the approach used on the modelling of the sub-layers, the cathode layer models were categorized into three groups, namely the diffusion approach, the partial-LTE approach and the hydrodynamic approach. The diffusion approach neglects the sheath and assumes that charge diffusion in the pre-sheath is the dominant cathode layer phenomenon promoting arc-cathode coupling. The partial-LTE approach considers the sheath and the thermal non-equilibrium (partial-LTE) in the pre-sheath but ignores diffusion. The hydrodynamic approach considers the sheath and models the pre-sheath including both thermal non-equilibria and species diffusion.

The existing results of the models applied to the study of GTAW were reviewed. The diffusion approach seems to be more accurate for evaluating the temperature fields in the plasma column while the hydrodynamic

approach is more accurate for predicting the arc voltage. The papers indicates that the hydrodynamic approach, as the most complete approach for describing the cathode layer, underestimates the temperature in the plasma. Therefore, in some literature the arc attachment is restricted in order to reproduce the plasma temperature with good agreement with experimental measurement.

Paper II

Modelling of electrode-arc coupling in electric arc welding

In Paper II a self-consistent cathode layer model with partial-LTE approach is tested in the frame of one-dimensional calculations. The current densities, energy fluxes and voltage drop within the sheath layer as well as the cathode surface temperature were studied for a range of current densities. It was shown that the cathode layer model provides results in good agreement with the available reference literature.

The model was applied to thoriated tungsten and pure tungsten cathode material. The effect of these two different cathode materials on the calculation results was discussed. The cathode layer model was coupled with the cathode and a plasma model in local thermal equilibrium. It was applied to a cylindrical cathode of 10 mm radius with planar end. In this case the electric conductive coupling applies to all the planar surface of the cathode end. The results obtained showed the potentiality of the model for gas tungsten arc applications.

Paper III

Coupling boundary for high-intensity electric arc attached on a non-homogeneous refractory cathode

The main focus of Paper III is on numerical calculation of implementing the cathode layer model as a coupling boundary condition. The numerical procedure for solving the cathode layer system of equations was described. The main equations and derivations were summarized and the iterative mechanism of solving different set of non-linear equations was given. The numerical procedure of coupling the cathode layer with the cathode and the plasma was also addressed. The emitter melting temperature, which represents inhomogeneity of the cathode, was introduced as the threshold of activating the cathode layer model. The paper described that the model

checks the threshold of the arc attachment at global iteration for each discrete element of the cathode surface. The cathode layer model then is activated or deactivated accordingly. The inhomogeneity of the cathode thus divides the cathode surface into two different regions, i.e. surface elements with and without arc attachment. Each region demands specific type of coupling boundary condition and the treatment of each region was described.

Paper III concluded that it is justified to neglect the space charge of emitted electrons when calculating the cathode surface electric field. The paper also verified that the Richardson-Dushman electron emission law supplemented with Schottky correction is used within its domain of validity when applied to GTA with a low work function emitter such as ThO_2.

Paper IV

Effect of cathode model on arc attachment for short high-intensity arc on a refractory cathode

In Paper IV a cathode layer model in the frame of partial-LTE approach was applied as an arc-cathode coupling boundary condition for GTA application modelled in OpenFOAM. Calculations were done for a 5 mm plasma arc at atmospheric pressure with a thoriated tungsten cathode with the arc current of 100 A and 200 A. The

The effect of the cathode surface heating by radiative absorption from the plasma and cooling by radiative emission was checked in the paper. Contrary to the assumption commonly made in GTA simulation, it was observed that cathode surface heating radiative cannot be considered negligible compared to cooling radiative. The paper also reported that both radiative absorption and emission of the cathode surface can be neglected compared to the other cathode surface heat fluxes.

The non-uniformity of the microstructure and composition of the cathode material, observed during high-intensity arc operation, described in Paper IV. Such inhomogeneity is due to the lower work function and lower melting temperature of the activators applied to the refractory cathode for stability purpose. The activators due to the lower melting temperature, melts and migrates towards the higher temperature region at the cathode tip. The activator has lower work function and thus is responsible for the electron emission. Therefore the inhomogeneous distribution of the emitter leads to inhomogeneous ability of the electrode to emit electrons. The inhomogeneity of the cathode material was introduced

to the cathode layer model as a criteria to restrict the arc attachment. Paper IV reported that the standard homogeneous cathode model overestimates the arc attachment on the cathode surface. It underestimates the cathode surface temperature measured close to the tip and also the plasma temperature measured in the plasma. However, the proposed non-homogeneous cathode model could restrict the arc attachment much closer to the experimental observation. It thus predicts the temperature profile of the cathode surface and plasma with a good agreement with experimental measurement.

References

[1] Electric glow discharge. http://www.plasma-universe.com/Electric_glow_discharge.

[2] N. A. Almeida, M. S. Benilov, and G. V. Naidis. Unified modelling of near-cathode plasma layers in high-pressure arc discharges. *Journal of Physics D: Applied Physics*, 41(24):245201, 2008.

[3] M Baeva, R Kozakov, S Gorchakov, and D Uhrlandt. Two-temperature chemically non-equilibrium modelling of transferred arcs. *Plasma Sources Science and Technology*, 21(5):055027, 2012.

[4] M. Baeva, D. Uhrlandt, M. S. Benilov, and M. D. Cunha. Comparing two non-equilibrium approaches to modelling of a free-burning arc. *Plasma Sources Science and Technology*, 22(6):065017, 2013.

[5] M. S. Benilov. Theory and modelling of arc cathodes. *Plasma Sources Science and Technology*, 11(3A):A49–A54, 2002.

[6] M. S. Benilov, M. Carpaij, and M. D. Cunha. 3D modelling of heating of thermionic cathodes by high-pressure arc plasmas. *Journal of Physics D: Applied Physics*, 39(10):2124–2134, 2006.

[7] M. S. Benilov, M. D. Cunha, and G. V. Naidis. Modelling interaction of multispecies plasmas with thermionic cathodes. *Plasma Sources Science and Technology*, 14(3):517–524, 2005.

[8] M. S. Benilov and A. Marotta. A model of the cathode region of atmospheric-pressure arcs. *Journal of Physics D-Applied Physics*, 28(9):1869–1882, 1995.

[9] Mikhail S Benilov. Near-cathode phenomena in HID lamps. *Industry Applications, IEEE Transactions on*, 37(4):986–993, 2001.

[10] MS Benilov. Understanding and modelling plasma–electrode interaction in high-pressure arc discharges: a review. *Journal of Physics D: Applied Physics*, 41(14):144001, 2008.

[11] M.I Boulos, P Fauchais, and E Pfender. *Thermal plasmas: fundamentals and applications*. Springer Science & Business Media, 2013.

[12] F Cayla. *Modélisation de l'interaction entre un arc électrique et une cathode*. PhD thesis, Université de Toulouse, Université Toulouse III-Paul Sabatier, 2008.

[13] F. Cayla, P. Freton, and J. J. Gonzalez. Arc/cathode interaction model. *Ieee Transactions on Plasma Science*, 36(4):1944–1954, 2008.

[14] RTC Choo, J Szekely, and RC Westhoff. Modeling of high-current arcs with emphasis on free surface phenomena in the weld pool. *Welding Journal*, 69(9):346–361, 1990.

[15] I. Choquet, P. Degond, and B. Lucquin-Desreux. A hierarchy of diffusion models for partially ionized plasmas. *Discrete and Continuous Dynamical Systems-Series B*, 8(4):735–772, 2007.

[16] I Choquet, A Javidi Shirvan, and H Nilsson. On the choice of electromagnetic model for short high-intensity arcs, applied to welding. *Journal of Physics D: Applied Physics*, 45(20):205203, 2012.

[17] I Choquet and B Lucquin-Desreux. Non equilibrium ionization in magnetized two-temperature thermal plasma. 2010.

[18] I Choquet, H Nilsson, Alireza Javidi Shirvan, and Nils Stenbacka. Numerical simulation of Ar-x CO2 shielding gas and its effect on an electric welding arc. In *IIW Commission XII/SG 212 Intermediate meeting, University West, TrollhÃ¤ttan, Sweden, 21-23 March 2011, IIW Doc. XII-2017-11*.

[19] S Coulombe. *A model of the electric arc attachment on non-refractory (cold) cathodes*. Phd thesis, 1997.

[20] S Coulombe and J Meunier. A comparison of electron-emission equations used in arc-cathode interaction calculations. *Journal of Physics D: Applied Physics*, 30(20):2905, 1997.

[21] S Coulombe and J Meunier. Thermo-field emission: a comparative study. *Journal of Physics D: Applied Physics*, 30(5):776, 1997.

[22] S. Coulombe and J. L. Meunier. Arc-cold cathode interactions: parametric dependence on local pressure. *Plasma Sources Science and Technology*, 6(4):508–517, 1997.

[23] C Delalondre. *Modélisation aérodynamique d arcs électriquesa fortes intensité avec prise en compte du déséquilibre thermodynamique local et du transfert thermiquea la cathode*. PhD thesis, 1990.

[24] P Freton, JJ Gonzalez, Z Ranarijaona, and J Mougenot. Energy equation formulations for two-temperature modelling of thermal plasmas. *Journal of Physics D: Applied Physics*, 45(46):465206, 2012.

[25] D. Godin and J. Y. Trepanier. A robust and efficient method for the computation of equilibrium composition in gaseous mixtures. *Plasma Chemistry and Plasma Processing*, 24(3):447–473, 2004.

[26] S Gorchakov, M Baeva, R Kozakov, D Uhrlandt, and T Schoenemann. Nonequilibrium arc model for the description of arcelectrode interaction. In *ICEC 2014; The 27th International Conference on Electrical Contacts; Proceedings of*, pages 1–6. VDE, 2014.

[27] GN Haddad and AJD Farmer. Temperature measurements in gas tungsten arcs. *Welding Journal*, 64(12):339–342, 1985.

[28] J Haidar. A theoretical model for gas metal arc welding and gas tungsten arc welding. i. *Journal of Applied Physics*, 84(7):3518–3529, 1998.

[29] J Haidar and AJD Farmer. Surface temperature measurements for tungsten-based cathodes of high-current free-burning arcs. *Journal of Physics D: Applied Physics*, 28(10):2089, 1995.

[30] Zh He and R Haug. Cathode spot initiation in different external conditions. *Journal of Physics D: Applied Physics*, 30(4):603, 1997.

[31] K. C. Hsu, K. Etemadi, and E. Pfender. Study of the free-burning high-intensity argon arc. *Journal of Applied Physics*, 54(3):1293, 1983.

[32] KC Hsu and E Pfender. Analysis of the cathode region of a free burning high intensity argon arc. *Journal of Applied Physics*, 54(7):3818–3824, 1983.

[33] KC Hsu and E Pfender. Two-temperature modeling of the free-burning, high-intensity arc. *Journal of applied physics*, 54(8):4359–4366, 1983.

[34] A Javidi Shirvan. *Modelling of Electric Arc Welding: arc-electrode coupling*. Thesis for the degree of Licentiate of Engineering 2013:12, ISSN 1652-8565, Chalmers University of Technology, 2013.

[35] A Kramida, Yu Ralchenko, J Reader, and NIST ASD Team. *NIST Atomic Spectra Database (ver. 5.0). http://physics.nist.gov/asd.* 2013.

[36] F. Lago, J. J. Gonzalez, P. Freton, and A. Gleizes. A numerical modelling of an electric arc and its interaction with the anode: Part i. the two-dimensional model. *Journal of Physics D: Applied Physics*, 37(6):883–897, 2004.

[37] TH Lee, AN Greenwood, and WD Breingan. A self consistent model for the cathode region of a high pressure arc. In *Proc. Seventh Int. Conf. Phenom. Ionized Gases*, volume 1, pages 670–680, 1966.

[38] He-Ping Li and M. S. Benilov. Effect of a near-cathode sheath on heat transfer in high-pressure arc plasmas. *Journal of Physics D: Applied Physics*, 40(7):2010–2017, 2007.

[39] S Lichtenberg, L Dabringhausen, O Langenscheidt, and J Mentel. The plasma boundary layer of hid-cathodes: modelling and numerical results. *Journal of Physics D: Applied Physics*, 38(17):3112–3127, 2005.

[40] J. J. Lowke, R. Morrow, and J. Haidar. A simplified unified theory of arcs and their electrodes. *Journal of Physics D-Applied Physics*, 30(14):2033–2042, 1997.

[41] Jr Messler and W Robert. *Principles of welding: processes, physics, chemistry, and metallurgy*. John Wiley & Sons, 2008.

[42] R Morrow and JJ Lowke. A one-dimensional theory for the electrode sheaths of electric arcs. *Journal of Physics D: Applied Physics*, 26(4):634, 1993.

[43] A B. Murphy, M Tanaka, K Yamamoto, Sh Tashiro, J J. Lowke, and K Ostrikov. Modelling of arc welding: The importance of including the arc plasma in the computational domain. *Vacuum*, 85(5):579–584, 2010.

[44] E. L. Murphy and R. H. Good. Thermionic emission, field emission, and the transition region. *Physical Review*, 102(6):1464–1473, 1956.

[45] V Nemchinsky. Erosion of thermionic cathodes in welding and plasma arc cutting systems. *Plasma Science, IEEE Transactions on*, 42(1):199–215, 2014.

[46] OH Nestor. Heat intensity and current density distributions at the anode of high current, inert gas arcs. *Journal of applied physics*, 33(5):1638–1648, 1962.

[47] AV Phelps and Z Lj Petrovic. Cold-cathode discharges and breakdown in argon: surface and gas phase production of secondary electrons. *Plasma Sources Science and Technology*, 8(3):R21, 1999.

[48] AV Potapov. Chemical equilibrium of multitemperature systems(law of mass action derivation of chemical equilibrium ionization of multitemperature system when electron and heavy particle temperature differ). *TEPLOFIZIKA VYSOKIKH TEMPERATUR*, 4:55–58, 1966.

[49] V. Rat, A. B. Murphy, J. Aubreton, M. F. Elchinger, and P. Fauchais. Treatment of non-equilibrium phenomena in thermal plasma flows. *Journal of Physics D: Applied Physics*, 41(18):183001, 2008.

[50] K-U Riemann. The bohm criterion and sheath formation. *Journal of Physics D: Applied Physics*, 24(4):493, 1991.

[51] A Sadek, M Ushio, and F Matsuda. Effect of rare earth metal oxide additions to tungsten electrodes. *Metallurgical Transactions A*, 21(12):3221–3236, 1990.

[52] L. Sansonnens, J. Haidar, and J. J. Lowke. Prediction of properties of free burning arcs including effects of ambipolar diffusion. *Journal of Physics D-Applied Physics*, 33(2):148–157, 2000.

[53] JA Sillero, D Ortega, E Munoz-Serrano, and E Casado. An experimental study of thoriated tungsten cathodes operating at different current intensities in an atmospheric-pressure plasma torch. *Journal of Physics D: Applied Physics*, 43(18):185204, 2010.

[54] M Tanaka, M Ushio, M Ikeuchi, and Y Kagebayashi. In situ measurements of electrode work functions in free-burning arcs during operation at atmospheric pressure. *Journal of Physics D: Applied Physics*, 38(1):29, 2005.

[55] M. van de Sanden and P. Schram. Generalized law of mass action for a two-temperature plasma. *Physical Review A*, 44(8):5150–5157, 1991.

[56] M. van de Sanden, P. Schram, A. Peeters, J. van der Mullen, and G. Kroesen. Thermodynamic generalization of the saha equation for a two-temperature plasma. *Physical Review A*, 40(9):5273–5276, 1989.

[57] K Weman. *Welding processes handbook*. Elsevier, 2011.

[58] J Wendelstorf. *Ab initio modelling of thermal plasma gas discharges (electric arcs)*. 2000.

[59] K Yamamoto, Si Tashiro, and M Tanaka. Numerical analysis of current attachment at thermionic cathode for gas tungsten arc at atmospheric pressure. *Transactions of JWRI*, 38(1):1–5, 2009.

[60] Stephen WH Yih and Chun T Wang. *Tungsten: sources, metallurgy, properties, and applications*. Plenum Publishing Corporation, 1979.

[61] X. Zhou and J. Heberlein. Analysis of the arc-cathode interaction of free-burning arcs. *Plasma Sources Science and Technology*, 3(4):564–574, 1994.

[62] X Zhou and J Heberlein. Characterization of the arc cathode attachment by emission spectroscopy and comparison to theoretical predictions. *Plasma chemistry and plasma processing*, 16(1):S229–S244, 1995.

[63] X Zhou, J Heberlein, and E Pfender. Theoretical study of factors influencing arc erosion of cathode. *Components, Packaging, and Manufacturing Technology, Part A, IEEE Transactions on*, 17(1):107–112, 1994.

[64] Peiyuan Zhu, JJ Lowke, and R Morrow. A unified theory of free burning arcs, cathode sheaths and cathodes. *Journal of Physics D: Applied Physics*, 25(8):1221, 1992.

[65] Peiyuan Zhu, JJ Lowke, R Morrow, and J Haidar. Prediction of anode temperatures of free burning arcs. *Journal of Physics D: Applied Physics*, 28(7):1369, 1995.

Appendices

A - Equations and derivations

Equations and derivations

All the derivations of the equations needed to obtain the cathode layer model are described in Section A-1. The governing equations in the cathode and plasma regions are reported in Section A-2.

A-1 Cathode layer model derivations

This section focuses on the cathode layer model, assuming that the plasma core can be described by a one-fluid model at LTE. The main elements of this model come from developments done by Cayla [12] based on former studies by Benilov and Marotta [8] and Zhou and Heberlein [61]. Minor changes were done, and they are indicated in the following section.

The cathode layer model includes the cathode sheath and the pre-sheath. It also takes into account the effect of the Knudsen layer. The model provides the information needed for coupling of energy and charge conservation between the plasma and the cathode. The cathode layer model is based on the main assumptions presented in Section A-1.1 The first step, described in Section A-1.2, consists in introducing the system of equations providing the plasma composition. The second step, described in Section A-1.3, consists in modelling the particle fluxes in the cathode sheath. Finally the model is closed in Section A-1.4 based on the basic physical principles of charge and energy conservations. The main outputs that are useful for the coupling with arc and cathode are the net heat flux to the cathode, $q^{cl\rightarrow c}$, the electron temperature at sheath/pre-sheath interface, $T_e^{s/ps}$ and heavy particle temperature at sheath/pre-sheath interface, $T_h^{s/ps}$. These outputs are used to set the energy and electric potential coupling boundary condition at the arc-cathode interface.

A-1.1 Main assumptions

The cathode layer model described in this appendix is based on the following main assumptions.
For the sheath:

- The emitted electrons are at thermal equilibrium with the cathode surface.
- The space charge of emitted electrons is neglected when calculating the cathode surface electric field [10].
- The cathode sheath is collisionless.
- The temperature of the back diffusion electrons is constant along the sheath and is equal to the electron temperature at the sheath/pre-sheath interface.
- The nearly isotropic distribution functions of the back diffusion electrons in the sheath can be approximated by a Maxwellian .
- All the ions reaching the cathode surface are recombined.

For the Knudsen layer:

- The ions leave the Knudsen layer and enter the sheath with the Bohm velocity [50].
- In the Knudsen layer, the component normal to the cathode wall of the ion distribution function can be approximated by an Heaviside distribution function defined based on Bohm velocity.

And for the pre-sheath layer:

- Real gas effect can be neglected in the pre-sheath since it is at pressure of the order of atmospheric pressure.
- Radiative ionization is negligible.
- The ionization energy is provided by the impacting electrons.
- The pre-sheath is assumed to be in static equilibrium.

A-1.2 Plasma composition in the pre-sheath

Two ionization processes can take place in a thermal plasma: impact ionization and radiative ionization. The former, dominant at atmospheric pressure, is the ionization process retained for modelling atmospheric welding arc [49]. In an argon plasma with temperature ranging from 300 to 30000K up to three ion species (Ar^{l+} with $l = 1, 2, 3$) present. The reactions taking place in the cathode layer are then the impact ionization reactions

$$Ar^{(l-1)+} + e \rightarrow Ar^{l+} + 2e \quad where \quad l = 1, 2, 3.$$

The incident electron is the particle provides the ionization energy. Electrons can indeed reach a high kinetic energy while accelerated by the electric field, contrary to the ions (due to their high inertial). The principle of detailed balance for this ionization process is described by the Saha equation. Different generalizations of the Saha equation exist for the two-temperature plasma of the pre-sheath. A review was done by Rat et al. [49]. Some cathode layer models [31, 58] are based on the Saha generalization developed by Potapov [48] to calculate the plasma composition. Nowadays this formulation is no longer used since it was shown to be incorrect from a thermodynamic point of view [56] as well as from a kinetic point of view [17]. Zhou and Heberlein [61], Coulombe and Meunier [22], and Cayla et al. [12, 13] used instead a formulation consistent with thermodynamics and kinetic theory: the formulation proposed by Van de Sanden et al. [56] based on the electron temperature. It is used in this study to calculate number density of the particles of argon plasma: $Ar, Ar^{+}, Ar^{2+}, Ar^{3+}, e^{-}$. To get these unknown parameters, five equations are needed. Three are provided by the Saha equation (for l= 1,2,3). In addition the Dalton's law and electrical neutrality are also needed to close the system.

Saha equations based on the electron temperature

The detailed balance is then given by the Saha law according to the Van de Sanden formulation [55, 56]. For $l = 1, 2, 3$ it is given as

$$\frac{n_e^{s/ps} n_{Ar^{l+}}^{s/ps}}{n_{Ar^{(l-1)+}}^{s/ps}} = 2\frac{Q_{Ar^{l+}}^{s/ps}}{Q_{Ar^{(l-1)+}}^{s/ps}} \frac{(2\pi m_e k_b T_e^{s/ps})^{\frac{3}{2}}}{h_p^3} \exp\left(-\frac{E_{i,Ar^{(l-1)+}} - \Delta E_l^{s/ps}}{k_b T_e^{s/ps}}\right), \quad \text{(A-1)}$$

where $n_{Ar}^{s/ps}$, $n_e^{s/ps}$ and $n_{Ar^{l+}}^{s/ps}$ respectively denote the number density of Ar atoms, electrons, and ions Ar^{l+} at the sheath/pre-sheath interface. h_p is the Planck constant, k_b the Boltzmann constant, m_e the electron mass, $E_{i,Ar^{(l-1)+}}$ the ionization energy of $Ar^{(l-1)+}$. $\Delta E_l^{s/ps}$ is the lowering of the ionization energy resulting from the Coulomb field applied by the surrounding charged particles. It is given by

$$\Delta E_l^{s/ps} = \frac{l e^2}{4\pi\epsilon_o \lambda_D}, \quad \text{(A-2)}$$

where λ_D is the Debye length

$$\lambda_D = \sqrt{\frac{\epsilon_o k_b}{e^2\left(n_e^{s/ps} T_e^{s/ps} + n_i^{s/ps} T_h^{s/ps}\right)}}. \quad \text{(A-3)}$$

$Q^{s/ps}_{Ar^{l+}}$ denotes the internal partition function of Ar^{l+} given by

$$Q^{s/ps}_{Ar^{l+}} = Q_{Ar^{l+}}(T_e^{s/ps}) = \sum_{j=1}^{J_{max}} g_j \exp(-\frac{\varepsilon_j}{k_b T_e^{s/ps}}), \tag{A-4}$$

where J_{max} is the number of discrete energy levels in the atom or ion Ar^{l+}, ε_j the energy of the discrete level j and g_j its degeneracy. The online toolbox of the National Institute of Standard and Technology [35] is employed to retrieve the J_{max}, ε_j and g_j data for argon atom and ions.

Dalton's law

According to Boulos et al. [11] real gas effects can be neglected in thermal arc at atmospheric conditions. The pressure in the pre-sheath is equal to the sum of the partial pressures of the individual gases, as stated by Dalton's law with partial pressures verifying the ideal gas law:

$$P = \sum_{l=0}^{3} n^{s/ps}_{Ar^{l+}} k_b T_h^{s/ps} + n_e^{s/ps} k_b T_e^{s/ps}, \tag{A-5}$$

where $T_h^{s/ps}$ is the heavy particles temperature (atoms and ions) at the sheath/pre-sheath interface. As the sheath is assumed to be collisionless the definition of the notion of temperature is problematic. Since the particles cannot exchange energy with each other while they move through a collisionless sheath, it is assumed [61] that the temperature of heavy particles is the same at the sheath/cathode interface and at the sheath/pre-sheath interface. Thus, $T^{c/s} = T_h^{s/ps} = T_i^{s/ps}$.

Electric neutrality

As the pre-sheath satisfies local electro-neutrality, the electron density in the pre-sheath and at the sheath/pre-sheath interface is equal to the sum of all the ion densities weighted by their ion charge l.

$$n_e^{s/ps} = \sum_{l=1}^{3} l\, n^{s/ps}_{Ar^{l+}}\,. \tag{A-6}$$

A-1.3 Flux components in the cathode layer

There are four main flux components in the cathode layer, i.e. the ion flux, the thermo-field emission flux, the secondary emission flux and the back diffusion electron flux.

Ion flux

The ions resulting from ionization in the pre-sheath (ionization layer) produce the ion flux towards the cathode surface which is given by

$$\varphi_i = n_i^{s/ps} v_B, \tag{A-7}$$

where $n_i^{s/ps}$ is the total ion number density at the sheath/pre-sheath interface,

$$n_i^{s/ps} = \sum_{l=1}^{3} n_{Ar^{l+}}^{s/ps}. \tag{A-8}$$

v_B is the Bohm velocity and it is given by

$$v_B = \sqrt{k_b \left(T_h^{s/ps} + Z T_e^{s/ps} \right) / m_i}, \tag{A-9}$$

where $Z = n_e^{s/ps} / n_i^{s/ps}$ is the average ion charge, and m_i the ion mass.

Back diffusion flux

The back diffusion flux is caused by electrons from the pre-sheath moving through the sheath towards the cathode. The distribution function of these electrons inside the sheath is Maxwellian,

$$f_e(y, v_x, v_y, v_z) = n_{es} \left(\frac{m_e}{2\pi k T_e} \right)^{3/2} \exp\left(\frac{-m_e (v_x^2 + v_y^2 + v_z^2)}{2 k T_e} \right), \tag{A-10}$$

where the y-direction is normal to the cathode surface and oriented towards the plasma. For back diffusion electrons, the sheath potential is repulsive. Only fast plasma electrons ($v_y \leq -\sqrt{2eU_s/m_e}$) can overcome this barrier. The flux of electrons to the cathode surface is thus

$$\begin{aligned} \varphi_{bd} &= \int_{v_x=-\infty}^{v_x=+\infty} \int_{v_y=-\infty}^{v_y=-\sqrt{2eU_s/m_e}} \int_{v_z=0}^{v_z=+\infty} v_y f_e(y, v_x, v_y, v_z) dv_x dv_y dv_z \\ &= \frac{n_e^{s/ps} v_e}{\sqrt{2\pi}} \exp\left(-\frac{eU^s}{k T_e^{s/ps}} \right), \end{aligned} \tag{A-11}$$

where U^s is the sheath voltage drop. The electron thermal velocity is given by

$$v_e = \sqrt{k_b T_e^{s/ps} / m_e}. \tag{A-12}$$

Secondary electron emission flux

When an ion colliding with the surface brings to the surface an energy larger than the work function, it can directly induce the emission of an electron. This is called the secondary electron emission (the primary emission is here the thermo-field emission). In the study by Lichtenberg et al. [39] the secondary emission current density φ_{sem} is proportional to φ_i ($\varphi_{sem} = \gamma\varphi_i$) while in the work by Cayla et al. [13] for the argon plasma it is simplified to $\varphi_{sem} = \gamma n_{Ar^+} v_s$. According to our investigation the value of φ_{sem} calculated by those two approaches are the same for argon plasma. However, this may not be valid for other types of plasma. Therefore, in this study the secondary electron emission current density is calculated as [39],

$$\varphi_{sem} = \gamma\, n_i^{s/ps} v_B, \tag{A-13}$$

where γ is the coefficient of secondary emission which depends on the plasma and cathode parameters. According to the study by Phelps and Petrovic [47] this coefficient is estimated to be equal to 0.1 for an argon plasma and a tungsten cathode.

Thermo-field electron emission flux

Conducting metals use to have one or two valence electrons per atom that are free to move between atoms. The minimum energy that must be given to a metal surface to liberate an electron is the work function. By absorption of sufficient thermal energy, a metal surface can emit electrons by thermoionic emission. The thermal energy is provided by the ions colliding with the surface. Thermo-field emission is the thermionic emission enhanced by the lowering of the surface potential barrier induced by the presence of the sheath adjacent to the cathode. Two different electron emission laws are used here.

The first variant is the flux of electron emission provided by the Richardson-Dushman model supplemented with the Schottky correction. It is given by

$$\varphi_{em}^{RD} = \frac{\lambda_R A_0 (T^{c/s})^2}{e} \exp\left(-\frac{\phi_{eff}}{k_b T^{c/s}}\right), \tag{A-14}$$

where $\phi_{eff} = \phi - \Delta\phi$ is the effective work function, ϕ the work function, and $\Delta\phi$ the Schottky correction. λ_R is a material specific factor, $A_0 = 4\pi m_e k_b^2 e/h_p^3$ the Richardson constant, e the electron elementary charge, and ϵ_o the permittivity of free space. The Schottky correction is written as

$$\Delta\phi = \sqrt{\frac{e^3 E^{c/s}}{4\pi\epsilon_o}}. \tag{A-15}$$

$E^{c/s}$ denotes the electric field produced at the cathode surface by the electrical space charge present in the cathode sheath layer. The electric field in the sheath derives from the electrostatic potential Φ produced by the sheath space charge. It can be derived from a one-dimensional and steady state approach if the plasma parameters across the sheath vary much faster than in the transverse direction. This simplification is justified in the sheath of usual welding arcs as their thickness uses to be much smaller than the characteristic cathode length. Φ can thus be obtained solving locally the 1-dimensional Poisson equation,

$$\varepsilon_0 \frac{d^2\Phi}{dy^2} = e(n_e^s - Z n_i^s), \tag{A-16}$$

where y is the direction normal to the cathode wall surface oriented from the wall towards the plasma, and n_e^s and n_i^s are the electron and ion number densities in the space charge layer. It can be noticed that the electrostatic potential Φ is equal to zero at the sheath/pre-sheath interface because of local electro-neutrality in the pre-sheath. To solve the Poisson equation A-16 the electron and ion charge density in the sheath are needed first to be determined. The sheath is assumed collisionless for both ions and electrons since its thickness is less than the ion and electron mean free path. The ion and electron distribution functions are thus governed by collisionless Boltzmann equations. For charged particles accelerated by an electric field along the y-direction, the steady and collisionless Boltzmann equation governing the distribution function $f = f(y, v_y)$ (with $f = f_i$ for ions and $f = f_e$ for electrons) writes

$$v_y \frac{\partial f}{\partial y} - \frac{q}{m}\frac{d\Phi}{dy}\frac{\partial f}{\partial v_y} = 0 \tag{A-17}$$

where v_y is the particle velocity along y, q the particle charge ($q = -e$ for electrons and eZ for ions), and m the particle mass ($m = m_e$ for electrons and m_i for ions). When the solution $f = f_e$ (resp. $f = f_i$) of equation A-17 is known, the electron (resp. ion) charge density along y is

$$n = n_{e(i)}(y) = \int_{-\infty}^{B_e(i)} f_{e(i)} dv_y \tag{A-18}$$

The upper limit of integration B_e for electrons and B_i for ions is described here. The ions present in the space charge layer come from the pre-sheath while the electrons should include both the back-diffusion electrons coming from the pre-sheath and the emitted electrons coming from the cathode surface. However, as proposed by Benilov [8] and checked in

Paper III, this last contribution can be neglected. The ion and electron distribution functions within the pre-sheath are Maxwellians at temperature T_i and T_e respectively since the pre-sheath satisfies partial LTE. The sheath electric field decelerates the back-diffusion electrons as they move toward the cathode, while it accelerates the positively charged ions. As a result, a large fraction of the back-diffusion electrons are reflected by the sheath potential barrier before reaching the cathode wall (and return to the pre-sheath) while the ions are accelerated up to collision with the cathode wall. It implies that the electron distribution function in the sheath can be assumed nearly isotropic in velocity, and approximated by a Maxwellian. It also implies that for electrons the upper limit of integration in equation A-18 is $B_e = +\infty$. The ions reach the cathode surface and are all assumed to recombine. As they do not travel back towards the pre-sheath (neutral atoms do instead), their sheath distribution function is highly non-isotropic in velocity and cannot be assumed Maxwellian. It also implies that for ions the upper limit of integration in equation A-18 is $B_i = 0$.

In the space charge layer, the electron distribution function f_e is Maxwellian since partial LTE is satisfied. The electron density in this region can then be calculated from the first moment of the Boltzmann equation A-17.

$$n_e = n_e(y) = n_e^s \exp(\frac{e\Phi}{kT_e}) \tag{A-19}$$

The ion density is more difficult to calculate as the ion distribution function f_i in the sheath is not known. The Boltzmann equation then needs to be solved. This requires knowing the boundary condition at the sheath/pre-sheath interface, $f_i(\infty, v_y)$. Riemann [50] showed that smooth matching of the pre-sheath and sheath solution f_i requires an additional transition layer called the Knudsen layer. The Knudsen layer is a thin sub-region of the pre-sheath next to the sheath and dominated by ion-ion collisions with no ionization [8]. The role of this sub-layer is to transform the ion distribution function from a Maxwellian function on the pre-sheath side to a distribution of forward-going particles on the sheath side. According to our knowledge, there is no known solution of the Knudsen layer model when ion-ion collisions are dominant. The following expression suggested by Benilov [8] is thus used:

$$f(\infty, v_y) = \begin{cases} \dfrac{n_i^{s/ps}}{2u_i^{s/ps}} & if \quad -(v_B - u_i^{s/ps}) > v_y > -(v_B + u_i^{s/ps}) \\ 0 & otherwise \end{cases} \tag{A-20}$$

where $n_i^{s/ps}$ is the ion number density at the sheath/pre-sheath interface and $u_i^{s/ps}$ is the thermal velocity of the ions at sheath/pre-sheath interface,

$$u_i^{s/ps} = \sqrt{\frac{k_b T_i^{s/ps}}{m_i}}. \tag{A-21}$$

It should be noticed that $Zn_i^{s/ps} = n_e^{s/ps}$ since the pre-sheath satisfies local electro-neutrality. The above expression for $f_i(\infty, v_y)$ reproduces the effect of the Knudsen layer in the sense that the velocity distribution of the ions leaving the pre-sheath through the ion Knudsen layer and entering the space charge layer describes forward-going ions. The lower and upper velocity bound $v_B - u_i^{s/ps}$ and $v_B + u_i^{s/ps}$ result from Bohm's criterion. As explained by Riemann [50], "Bohm's criterion expresses a necessary condition for the formation of a stationary sheath in front of a negative absorbing wall". The change of variable v_y to $1/2m_i v_y^2 + Ze\varphi$ allows obtaining the following ion distribution function $f_i(y, v_y)$ solution of equation A-17 [8]

$$f_i(y, v_y) = \begin{cases} \dfrac{n_i^{s/ps}}{2u_i^{s/ps}} & if \quad -v_- > v_y > -v_+ \\ 0 & otherwise \end{cases} \tag{A-22}$$

Here v_+ and v_- respectively denote the maximum and the minimum ion velocity allowing satisfying Bohm's criterion for the sheath voltage drop U^s given by

$$v_\pm = \sqrt{\left(v_B \pm u_i^{s/ps}\right)^2 + 2eZU^s/m_i}. \tag{A-23}$$

The ion density in the space charge layer can then be calculated from equation A-18, leading to

$$n_i^s = n_i^{s/ps} \frac{v_+ - v_-}{2u_i^{s/ps}}. \tag{A-24}$$

After substitution of n_e^s and n_i^s using the relations A-19 and A-24 in the one-dimensional Poisson equation A-16 and integration, the electric field at the cathode surface $E^{c/s}$ can be expressed by setting Φ to the sheath voltage drop U^s. It is given by

$$E^{c/s} = \sqrt{\frac{2n_i^{s/ps}}{\epsilon_o}\left[m_i\left(\frac{v_+^3 - v_-^3}{6u_i^{s/ps}} - v_B^2 - \frac{1}{3}u_i^{s/ps\,2}\right) - Zk_bT_e^{s/ps}\left(1 - \exp(-\frac{eU^s}{k_bT_e^{s/ps}})\right)\right]}. \tag{A-25}$$

The second alternative of the electron emission law was developed by Murphy and Good [44]. It is given by

$$\varphi_{em}^{MG} = \frac{4\pi m_e k_B T^{c/s}}{h^3} \int_{-\infty}^{W_l} \ln\left[1+\exp\left(-\frac{W+e\phi}{k_B T^{c/s}}\right)\right]\left[1+\exp\left(\frac{a\,v(y)}{y^{3/2}}\right)\right]^{-1} dW + \frac{4\pi m_e k_B T^{c/s}}{h^3} \int_{W_l}^{\infty} \ln\left[1+\exp\left(-\frac{W+e\phi}{k_B T^{c/s}}\right)\right] dW, \tag{A-26}$$

where

$$W_l = -\sqrt{\frac{e^3 E^{c/s}}{8\pi\epsilon_o}}, \quad a = \frac{4\sqrt{2}}{3(4\pi\epsilon_0)^{3/4}}\left(\frac{m_e^2 e^5}{\hbar^4 E^{c/s}}\right)^{1/4}, \quad y = \sqrt{\frac{e^3 E^{c/s}}{4\pi\epsilon_o}}\frac{1}{|W|},$$

where $\hbar = h/(2\pi)$ and

$$v(y) = \begin{cases} \sqrt{\frac{y}{2}}\left[2E\left(\frac{y-1}{2y}\right) - (y+1)K\left(\frac{y-1}{2y}\right)\right] & if \quad y > 1 \\ \sqrt{1+y}\left[2E\left(\frac{1-y}{1+y}\right) - yK\left(\frac{1-y}{1+y}\right)\right] & if \quad y < 1 \end{cases}$$

$K = K(m)$ and $E = E(m)$ are the complete elliptic functions of first and second kind defined by

$$K(m) = \int_0^{\pi/2} \left(1 - m\sin^2\theta\right)^{-1/2} d\theta \quad \text{and} \quad E(m) = \int_0^{\pi/2} \left(1 - m\sin^2\theta\right)^{1/2} d\theta. \tag{A-27}$$

A-1.4 Charge and energy conservation

To close the cathode layer model a system of three more equations is needed. These equations are the current and energy balance at the cathode surface as well as the energy balance within the pre-sheath layer.

Current conservation at the cathode/sheath interface

The current conservation at the cathode surface expresses

$$j^{c/s} = e(Z\varphi_i + \varphi_{em} + \varphi_{sem} - \varphi_{bd}), \tag{A-28}$$

where $j^{c/s}$ is the cathode current density at the cathode surface.

Energy balance at the cathode/sheath interface

The energy conservation at the cathode surface implies that the net heat flux from the cathode layer to the cathode, $q^{cl\to c}$, is balanced by the heat flux conducted into the cathode, as

$$q^{cl\to c} = -\kappa^c \nabla T^c. \tag{A-29}$$

κ^c denotes the cathode thermal conductivity, ∇T^c the cathode temperature gradient at the surface. $q^{cl\to c}$ can be calculated as

$$q^{cl\to c} = q_i^{cl\to c} + q_{bd}^{cl\to c} - q_{em}^{c\to cl} - q_{sem}^{c\to cl} - q_a^{c\to cl} + q_{rad}^{abs} - q_{rad}^{em}, \tag{A-30}$$

where $q_i^{cl\to c}$ and $q_{bd}^{cl\to c}$ are respectively the ion energy flux and the back diffusion electron energy flux from the cathode layer to the cathode surface. $q_{em}^{c\to cl}$, $q_{sem}^{c\to cl}$ and $q_a^{c\to cl}$ are respectively the thermo-field electron emission, the secondary electron emission and the recombined ion energy flux from the cathode surface to the cathode layer. q_{rad}^{abs} and q_{rad}^{em} are respectively the radiative absorption from the plasma and the radiative emission at the cathode surface.

Radiative cooling and heating

The radiation heat flux emitted locally by the cathode surface is expressed using the gray body model

$$q_{rad}^{em} = q_{rad}^{em}(T^{c/s}) = \epsilon\,\sigma\,(T^{c/s})^4 \tag{A-31}$$

where σ is the Stefan-Boltzmann constant, ϵ the cathode material emissivity. For tungsten the dimensionless emissivity can be written as [60]

$$\epsilon = \epsilon(T^{c/s}) = -0.0266 + 1.8197\times10^{-4}(T^{c/s}) - 2.1946\times10^{-8}(T^{c/s})^2, \tag{A-32}$$

where the local cathode surface temperature $T^{c/s}$ is in Kelvin. The radiation heat flux absorbed locally by the cathode from the plasma bulk of volume V is approximated using the view factor method [14, 36, 42],

$$q_{rad}^{abs} = \int_V \frac{S_{rad}}{4\pi r_{ij}^2}\cos\psi\, dV_j, \tag{A-33}$$

where S_{rad} is the radiative loss of the differential plasma volume dV_j. S_{rad} is calculated from the net emission coefficient used in the thermal plasma model. r_{ij} represents the distance between the differential area i of the cathode surface and each differential volume j of the plasma, and ψ is the

view factor angle between the elements i and j.

Ion heating

The energy flux of ions towards the cathode $q_i^{cl\to c}$ includes the kinetic energy brought to the cathode surface by the ions $(q_{KE})_i$, and the energy released to the surface by ion neutralization $(q_{ion})_i$. The flux of ions kinetic energy towards the cathode (along y-direction) is by definition

$$(q_{KE})_i = \int_{v_x=-\infty}^{v_x=+\infty} \int_{v_y=-\infty}^{v_y=0} \int_{v_z=-\infty}^{v_z=+\infty} \frac{1}{2} m_i (v_x^2 + v_y^2 + v_z^2) v_y f_i(y, v_x, v_y, v_z) dv_x dv_y dv_z. \tag{A-34}$$

As partial-LTE is satisfied in the pre-sheath, the velocity distribution of ions entering the sheath obeys a Maxwellian distribution at the temperature $T_i = T^{c/s}$. Only ions with kinetic energy large enough can cross the space charge layer and reach the cathode surface. Therefore, the ion velocity distribution along the y-direction needs to be truncated to retain only ions with a large enough velocity u_y. Thus the motion of the ions in the y-direction is not chaotic and the distribution in this direction cannot be Maxwellian. The ion distribution function $f_i(y, v_x, v_y, v_z)$ is equal to $f_i(y, v_y) f_M(v_x) f_M(v_z)$ where $f_i(y, v_y)$ is defined by equation A-22 and f_M denotes a standard Maxwellian distribution function. Then

$$f_i(y, v_x, v_y, v_z) = \begin{cases} \dfrac{n_i^{s/ps}}{4\pi (u_i^{s/ps})^3} \exp\Big(- \dfrac{v_x^2 + v_z^2}{2 (u_i^{s/ps})^2} \Big) & if \quad -v_- > v_y > -v_+ \\ 0 & otherwise \end{cases} \tag{A-35}$$

After integration, equations A-34 and A-35 lead to

$$(q_{KE})_i = n_i^{s/ps} v_B \Big(m_i (u_i^{s/ps})^2 + \frac{1}{2} m_i v_B^2 + \frac{1}{2} m_i u_i^2 + Ze\Phi \Big) \tag{A-36}$$

The first term on the right hand side $n_i^{s/ps} v_B$ is the ion flux, φ_i. The first term in bracket represents the average ion kinetic energy along the x- and z-direction, as expected for a Maxwellian distribution. The three last terms in bracket do represent the average ion kinetic energy along the y-direction. It differs very significantly from the kinetic energy, $1/2kT_i$, a Maxwellian distribution would provide. The reasons are the following. The ion velocities along the y-direction are mono-directional, so restricted to $v_y \leq 0$. Their distribution is truncated to satisfy Bohm criteria. Finally

the ion velocities are also accelerated by the electrostatic potential (in the sheath, $\Phi = U^s$).

The energy released to the surface by ion neutralization with cathode electrons is

$$(q_{ion})_i = \varphi_i(\bar{E}_i - Z\phi_{eff}). \tag{A-37}$$

where $Z\phi_{eff}$ is the energy required to take recombination electrons from the cathode surface. $\bar{E}_i$ is the average energy of ion recombination at the cathode surface. It is given by

$$\bar{E}_i = \sum_{l=1}^{3} n^{ps/s}_{Ar^{l+}} E_{i,Ar^{l+}}, \tag{A-38}$$

where $E_{i,Ar^{l+}}$ is the ionization energy of the reaction $Ar^{(l-1)+} + e \rightarrow Ar^{l+} + 2e$. Finally the total ion energy flux to the cathode is given by

$$q_i^{cl\rightarrow c} = \varphi_i \left(\overbrace{2kT_i^{s/ps} + \frac{kZT_e^{s/ps}}{2} + ZeU^s}^{kinetic\ energy} + \overbrace{\bar{E}_i - Z\phi_{eff}}^{ion\ neutralization} \right). \tag{A-39}$$

This expression was obtained assuming that all the ions recombined with cathode electrons. However, ions also recombined with the back diffusion electrons that reach the cathode surface. This recombination is considered in the back diffusion heating.

Back diffusion heating

The electrons coming from the pre-sheath with a velocity large enough ($v_y \leq -\sqrt{\frac{2eU^s}{m_e}}$) can pass the sheath voltage drop, and reach the cathode surface. This produces a flux of energy to the cathode

$$q_{bd}^{cl\rightarrow c} = \varphi_{bd} \left(\phi_{eff} + 2k_b T_e^{s/ps} \right). \tag{A-40}$$

The back diffusion electrons reaching the cathode surface recombine with ions. The first term on the right hand side is thus a correction for equation (A-39). It indicates when an ion recombined with a back diffusion electron rather than a cathode electron, there is no need to provide the energy ϕ_{eff}.

Electron emission cooling

The electrons emitted, either by thermo-field emission or by secondary

emission, transfer their energy from the cathode surface to the sheath, according to

$$q_{em}^{c\to cl} = \varphi_{em}\left(\phi_{eff} + 2k_b T^{c/s}\right), \tag{A-41}$$

$$q_{sem}^{c\to cl} = \varphi_{sem}\left(\phi_{eff} + 2k_b T^{c/s}\right). \tag{A-42}$$

The first contribution to the energy transferred from the cathode by electrons is the effective work function. The second contribution is the kinetic energy of electrons. It is obtained assuming that the electrons are at thermal equilibrium with the cathode surface when emitted ($T_e = T^{c/s}$). Their distribution function is a Maxwellian reduced to half the velocity space concerning the y-direction.

Recombined ion cooling

The ions reaching the cathode surface recombine and may go back towards the plasma. This forms a cooling heat flux by recombined atoms. Based on the assumption that all of the ions are neutralized at the cathode surface, and that the resultant atoms are at thermal equilibrium with the cathode surface, this cooling heat flux is equal to

$$q_a^{c\to cl} = \varphi_i\left(2k_b T^{c/s}\right). \tag{A-43}$$

Considering equations A-30 to A-43, the net heat flux to the cathode surface is given by

$$\begin{aligned} q^{cl\to c} = {} & \varphi_i\left(\tfrac{1}{2}Zk_bT_e^{s/ps} + eZU^s + \bar{E}_i - Z\phi_{eff}\right) - (\varphi_{em} + \varphi_{sem})\left(\phi_{eff} + 2k_bT^{c/s}\right) \\ & + \varphi_{bd}\left(\phi_{eff} + 2k_bT_e^{s/ps}\right) - q_{rad}^{em} + q_{rad}^{abs}. \end{aligned} \tag{A-44}$$

Energy balance in the pre-sheath

The energy balance in the pre-sheath implies that the net heat flux leaving the pre-sheath through the sheath/pre-sheath and the pre-sheath/plasma interfaces is balanced by the work done by the electric field on the charged particles moving through the pre-sheath. It is given by

$$q_i^{ps\to s} + q_{bd}^{ps\to s} + q_e^{ps\to p} - (q_{em}^{s\to ps} + q_{sem}^{s\to ps}) = W_E^{ps}, \tag{A-45}$$

where $q_i^{ps\to s}$ and $q_{bd}^{ps\to s}$ are respectively the ion and the back diffusion energy flux from the pre-sheath to the sheath. $q_e^{ps\to p}$ is the energy flux of the electrons leaving the pre-sheath towards the plasma. $q_{em}^{s\to ps}$ and $q_{sem}^{s\to ps}$ are respectively the energy transferred to the pre-sheath by the thermo-field

and secondary electron emission. W_E^{ps} is the average work of the electric field over the electrons inside the pre-sheath.

Ionization cooling

Ionization cooling includes two components. The first one corresponds to the ionization energy sink. The ionization energy sink is $\varphi_i \bar{E}_i$ with $\bar{E}_i$ defined in equation A-38. The second component is the energy transported away by the ions as they move towards the sheath. It is defined in equation A-36. At the sheath/pre-sheath interface $\Phi = 0$ because of local electro-neutrality so that $(q_{KE})_i = \varphi_i(2k_b T_i^{s/ps} + \frac{k_b Z T_e^{s/ps}}{2})$. As a result the total cooling in the pre-sheath because of ionization is

$$q_i^{ps\to s} = \varphi_i \left(2k_b T_i^{s/ps} + \frac{kZ T_e^{s/ps}}{2} + \bar{E}_i \right). \tag{A-46}$$

Electron emission heating

The electrons emitted by thermo-field and by secondary emission are assumed to be at thermal equilibrium with the cathode surface when emitted. They are accelerated in the sheath by the sheath voltage drop and they thus bring the following energy flux to the pre-sheath:

$$q_{em}^{s\to ps} = \varphi_{em} \left(2k_b T^{c/s} + eU^s \right), \tag{A-47}$$

$$q_{sem}^{s\to ps} = \varphi_{sem} \left(2k_b T^{c/s} + eU^s \right). \tag{A-48}$$

The first term in bracket is the thermal energy of the electrons moving from the cathode. The second term refers to the work done on the electrons by the sheath voltage drop U^s.

Back diffusion cooling

Back diffusion electrons which have enough energy can leave the pre-sheath, pass the potential barrier of the sheath layer and reach the cathode. The flux of energy carried away by these electrons is described by

$$q_{bd}^{ps\to s} = \varphi_{bd} \left(2k T_e^{s/ps} + eU^s \right). \tag{A-49}$$

The first term in the bracket is the thermal energy of the electrons and the second term refers to the fact that the electrons with the kinetic energy

eU^s are able to go through the sheath potential barrier towards the cathode.

Work of electric field

The emitted electrons leave the sheath and enter the pre-sheath with the net flux of $\varphi_{em} + \varphi_{sem} - \varphi_{bd}$ and move away from the pre-sheath towards the plasma with the flux of $\varphi_{tot} = j^{c/s}/e$. The average current density across the pre-sheath is thus $\frac{1}{2}(\varphi_{em} + \varphi_{sem} - \varphi_{bd} + \varphi_{tot})$. These electrons move in an electric field produced by the pre-sheath voltage drop U^i. They thus produce an average work defined by

$$W_E^{ps} = \frac{e(\varphi_{sem} + \varphi_{em} - \varphi_{bd} + \varphi_{tot})}{2} U^i \tag{A-50}$$

where U^i is the voltage drop in the pre-sheath. It can be described as follows [8]:

$$U^i = \frac{kT_e^{s/ps}}{e} \ln \frac{n_e^{p/ps}}{n_e^{s/ps}}, \tag{A-51}$$

The expression A-51 was obtained by Benilov and Marotta [8] using an estimation of the ion number density at the sheath/pre-sheath interface. This estimation can be used when the ionization degree of the pre-sheath is between about 0.6 to 1 ($T_e \geq 15000K$). According to Benilov and Marotta [8], at lower ionization degree the pre-sheath cannot remain in static equilibrium. However, this non-equilibrium effect is not taken into account when $\alpha < 0.6$, and equation A-51 is used for any ionization degree.

Electron cooling

According to Benilov and Marotta [8] the flux of the energy carried away by the electrons leaving the pre-sheath to the bulk plasma is equal to

$$q_e^{ps \to p} = 3.2 e j^{c/s} k T_e^{s/ps} \tag{A-52}$$

The coefficient 3.2 includes two contributions. A factor 2.5 accounting for enthalpy transport resulting from the electric current. The rest is a thermal-diffusion coefficient calculated for a strongly ionized plasma [8].

Considering Equations A-45 to A-52 the energy balance in the pre-

sheath layer can be rewritten as

$$\begin{aligned}(\varphi_{em}+\varphi_{sem})\left(2kT^{c/s}+eU^{s}+kT_e^{s/ps}\left(\ln\frac{n_e^{p/ps}}{n_e^{s/ps}}-3.2\right)\right)\\ =\varphi_{bd}\left(eU^{s}+kT_e^{s/ps}\left(\ln\frac{n_e^{p/ps}}{n_e^{s/ps}}-1.2\right)\right)\\ +\varphi_i\left(2kT_i^{s/ps}+\bar{E}_i+ZkT_e^{s/ps}\left(3.7-0.5\ln\frac{n_e^{p/ps}}{n_e^{s/ps}}\right)\right).\end{aligned} \tag{A-53}$$

A-2 Equations governing the cathode and the plasma

The steady state energy conservation equation governing the cathode temperature T^c is written as

$$\nabla\cdot(\kappa^c\,\nabla T^c)=\mathbf{j}\cdot\mathbf{E}. \tag{A-54}$$

The Joule heating term, on the right hand side depends on the current density $\mathbf{j}$ and the electric field $\mathbf{E}$. The plasma is governed by a thermo-fluid model applied to a Newtonian fluid assuming a one-fluid model in local thermal equilibrium, a thermally expansible and mechanically incompressible fluid, and a steady-state and laminar flow. In the framework of these assumptions the mass, momentum and energy conservation equations in the plasma at steady state are given by

$$\nabla\cdot(\rho\mathbf{u})=0, \tag{A-55}$$

$$\nabla\cdot(\rho\mathbf{u}\otimes\mathbf{u})-\nabla\cdot\left[\mu\left(\nabla\mathbf{u}+(\nabla\mathbf{u})^T\right)-\tfrac{2}{3}\mu(\nabla\cdot\mathbf{u})\mathbf{I}\right]=-\nabla P+\mathbf{j}\times\mathbf{B}, \tag{A-56}$$

$$\nabla\cdot(\rho\mathbf{u}h)-\nabla\cdot(\frac{\kappa^p}{C_p}\nabla h)=\mathbf{u}\cdot\nabla P+\mathbf{j}\cdot\mathbf{E}-Q_{rad}+\nabla\cdot\left[\frac{5\,k_b\,\mathbf{j}\,h}{2\,e\,C_p}\right]. \tag{A-57}$$

$\rho=\rho(T^p)$ denotes the plasma density, $\mathbf{u}$ the velocity, P the pressure, h the specific enthalpy, T^p the plasma temperature, $\mu=\mu(T^p)$ the viscosity, $\mathbf{I}$ the identity tensor, and $\mathbf{B}$ the magnetic field. $\kappa^p=\kappa_p(T^p)$ is the thermal conductivity, $Q_{rad}=Q_{rad}(T^p)$ the radiation heat loss and $C_p=C_p(T^p)$ the specific heat at constant pressure.

The electromagnetic part of the model is similar for the cathode and the thermal plasma. It is derived from Maxwell equations supplemented

with Ohm's law [16]. Using Laurentz gauge, it simplifies to the scalar Poisson equation governing the electric potential V given by

$$\nabla\cdot(\sigma\ \nabla V) = 0, \tag{A-58}$$

supplemented with a vectorial Poisson equation governing the magnetic potential **A**, given by

$$\triangle\mathbf{A} = \mu_o\ \sigma\ \nabla V. \tag{A-59}$$

μ_o is the permeability of free space and σ is the electric conductivity. It is set to $\sigma_p(T_p)$ in the thermal plasma, and to $\sigma_c(T_c)$ in the cathode. The current density **j**, the magnetic field **B** and the electric field **E** are derived from the magnetic and the electric potentials according to

$$\mathbf{j} = \sigma\ \mathbf{E}, \tag{A-60}$$

$$\mathbf{B} = \nabla\times\mathbf{A}, \tag{A-61}$$

$$\mathbf{E} = -\nabla V. \tag{A-62}$$